UCLA
UCLA Previously Published Works

Title

Co-imaging of RelA and c-Rel reveals features of NF-κB signaling for ligand discrimination.

Permalink

Journal

Authors

Rahman, Shah

Singh, Apeksha

Lowe, Sarina

et al.

Publication Date

DOI

Peer reviewed

Co-imaging of RelA and c-Rel reveals features of NF-κB signaling for ligand discrimination

Shah Md Toufiqur Rahman[1], **Apeksha Singh**[2], **Sarina Lowe**[2], **Mohammad Aqdas**[1], **Kevin Jiang**[2], **Haripriya Vaidehi Narayanan**[2], **Alexander Hoffmann**[2], **Myong-Hee Sung**[1,3,*]

[1]Laboratory of Molecular Biology and Immunology, National Institute on Aging, National Institutes of Health, Baltimore, MD 21224, USA

[2]Institute for Quantitative and Computational Biosciences and Department of Microbiology, Immunology, and Molecular Genetics, University of California, Los Angeles, Los Angeles, CA, USA

[3]Lead contact

SUMMARY

Individual cell sensing of external cues has evolved through the temporal patterns in signaling. Since nuclear factor κB (NF-κB) signaling dynamics have been examined using a single subunit, RelA, it remains unclear whether more information might be transmitted via other subunits. Using NF-κB double-knockin reporter mice, we monitored both canonical NF-κB subunits, RelA and c-Rel, simultaneously in single macrophages by quantitative live-cell imaging. We show that signaling features of RelA and c-Rel convey more information about the stimuli than those of either subunit alone. Machine learning is used to predict the ligand identity accurately based on RelA and c-Rel signaling features without considering the co-activated factors. Ligand discrimination is achieved through selective non-redundancy of RelA and c-Rel signaling dynamics, as well as their temporal coordination. These results suggest a potential role of c-Rel in fine-tuning immune responses and highlight the need for approaches that will elucidate the mechanisms regulating NF-κB subunit specificity.

Graphical abstract

*Correspondence: sungm@nih.gov.
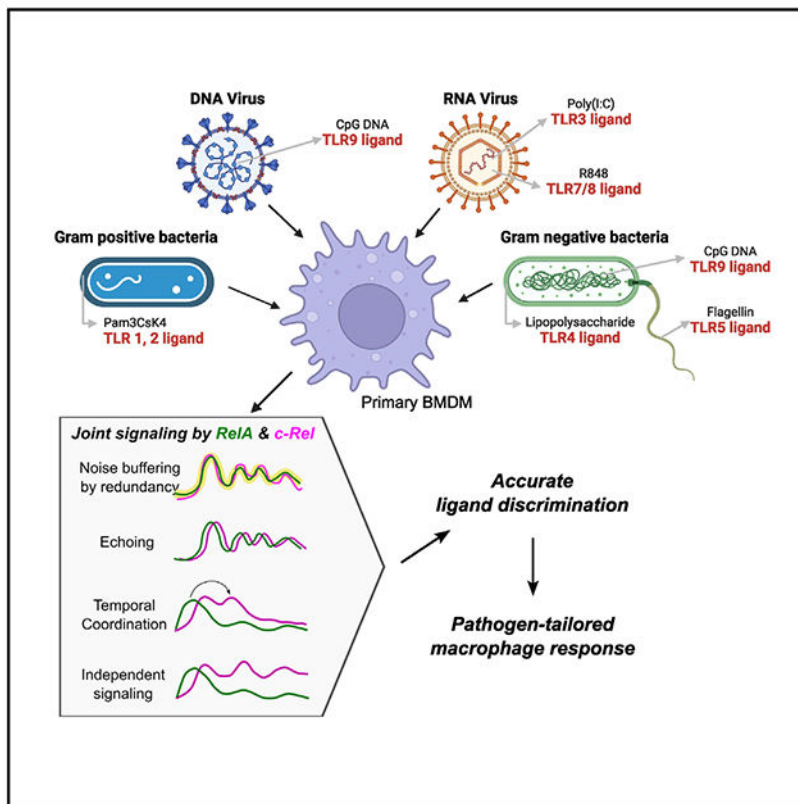
In brief

Rahman et al. perform quantitative livecell imaging of macrophages from NF-κB double-knockin reporter mice and show that both RelA and c-Rel subunits contribute to accurate discrimination of pathogen-derived ligands. Signaling features of the two NF-κB subunits are temporally coordinated and non-redundant in individual cells.

INTRODUCTION

Individual cells make irreversible fate decisions based on information received through the milieu of hormones, cytokines, metabolites, and biochemical input from direct cell-cell contacts. The information content and the accuracy of single cells interpreting the input have been a topic of fundamental importance.[1] While early studies of snapshot measurements reported the limited information capacity of individual single cells,[2] recent studies have shown various mechanisms of augmented information processing capacity, including combined signaling of two pathways,[3] time integration of signaling,[4] and dynamic response patterns.[5–8] For a ubiquitous immune transcriptional regulator such as nuclear factor κB (NF-κB), it is especially important to understand the information coding capacity, because of its wide-ranging involvement in numerous cell decision-making processes, and the broad implications.[9–14]

NF-κB proteins mediate much of the canonical signaling directly downstream of a wide range of microenvironmental cues in immune cell communications.[13,15–17] Foundational

studies have shown how NF-κB signaling dynamics can regulate gene expression in response to extracellular signals, mainly using engineered cell lines expressing a transgene that encodes a fluorescent fusion of the RelA (also known as p65) subunit of NF-κB.[18–29] Recent advances in experimental approaches have provided a more functionally relevant characterization of NF-κB dynamics in primary cells in terms of "signaling codons," i.e., dynamical features of signaling that convey information about ligand identity, using fluorescent knockin (KI) reporter mouse macrophages.[7]

However, existing data are limited to the RelA subunit of the NF-κB/Rel family, whereas both RelA and another transcriptionally active subunit, c-Rel, produce heterodimers and homodimers that mediate the canonical pathway activities. Although both NF-κB subunits share upstream signaling cascades and have similar domains and structures,[30] their biological functions have diverged significantly. The most striking difference is that the RelA knockout (KO) is embryonic lethal due to massive tumor necrosis factor alpha (TNF-α)-induced liver apoptosis,[31,32] whereas c-Rel deficiency leads to limited defects in T and B cells.[33–35] On the other hand, the induction of inflammatory gene expression was largely preserved in fibroblasts and macrophages from *Rel* (encoding c-Rel) KO mice.[36,37] Nonetheless, the results of conventional KO experiments are subject to compensation by family members such as RelA and are limited to the chosen assays, time points, cell types, and technical challenges. Therefore, we sought to understand if and how RelA and c-Rel signaling activities are coordinated in individual cells using quantitative live-cell analyses.

Macrophages are innate immune cells that respond to environmental signals such as foreign agents or *in vivo* damage products, thereby serving as a model cell context where NF-κB signaling can convey biological information for functional responses.[38] While much has been learned about chromatin regulatory mechanisms and the impact of tissue-specific niches in macrophage biology, predictive quantitative models are necessary to understand how they mount proper functional responses to a wide variety of pathogen-associated molecular patterns (PAMPs).

Here, we used the recently developed double-KI (DKI) reporter mice[39] and assessed how primary macrophages interpret diverse pathogenic and host signals through quantitative features of RelA and c-Rel. We found that c-Rel augments the ligand discrimination capability of macrophages beyond what is possible through RelA alone. Mathematical modeling suggested that the biochemical characteristics of RelA and c-Rel interactions account for their distinct dynamics and their coordination in individual macrophage responses. Our quantitative approaches provide an unprecedented insight about how macrophages exploit coordinated or independent actions of RelA and c-Rel signaling features to discriminate ligand identity.

RESULTS

Simultaneous quantitative imaging of NF-κB RelA and c-Rel in live primary macrophages captures the subunit-specific signaling features

To monitor the endogenous activity of both subunits of NF-κB in primary macrophages, we isolated bone-marrow-derived macrophages (BMDMs) from our NF-κB DKI reporter

mice, homozygous for mEGFP-RelA and for mScarlet-c-Rel.[39] The DKI mice allow simultaneous visualization of endogenous RelA and c-Rel in the same cell. For a systematic profiling of the ligand-specific NF-κB activation dynamics, BMDMs were stimulated with six different Toll-like receptor (TLR) ligands (representing various PAMPs) along with a pro-inflammatory cytokine, TNF-α. Cells were stained with a far-red, live-cell dye, SPY650-DNA, for nuclear segmentation, which allows us to perform long-term live imaging without phototoxicity. We then carried out quantitative long-term livecell imaging of DKI mouse BMDMs using our custom time-lapse microscopy and automated image analysis workflow (Figures 1 and S1), and single-cell RelA and c-Rel signaling was assessed by the nuclear:total ratio of their mean fluorescence intensities.

The single-cell trajectories for ligand-activated RelA and c-Rel responses in primary BMDMs showed noticeable ligand-specific patterns for both subunits, with c-Rel often reaching higher nuclear translocation peaks (Figure 2). These patterns contrast with the previously published data from immortalized macrophages (RAW267.4 cells stably expressing the fluorescent fusion RelA or c-Rel proteins).[40] The primary macrophage cells showed generally stronger and more sustained responses with clearly ligand-specific response times (Figure 2A), compared to the immortalized macrophages stimulated with the same ligand doses.[40] For example, the immortalized macrophages had little or no NF-κB activation after flagellin, CpG, or TNF-α treatment, whereas the primary BMDMs show activation of both RelA and c-Rel in response to the same concentrations of stimulating ligands. Overall, NF-κB signaling responses in BMDMs were robust, with temporal patterns that appear to reflect ligand specificity.

Since co-imaging of RelA and c-Rel in live cells has no precedent, immediate attention was given to a careful comparison of the single-cell signaling trajectories for RelA and c-Rel. Despite the different phenotypes of genetic KOs, the two subunits are both mediators of canonical NF-κB responses. We asked whether c-Rel follows similar signaling dynamics to RelA after activation by the ligands in terms of the following quantitative features extracted from the single-cell trajectories: the peak amplitude, the time to first peak, the area under the curve (AUC), the duration of signaling, the slope of the first rise, the post-peak attenuation rate, and, for oscillatory trajectories, the number of periodic cycles and the period of oscillation (Figure 2B).

For all the TLR ligands, the amplitude of c-Rel was higher than that of RelA (in the nuclear/total ratio scale, which allows comparison of the two imaging channels), consistent with data that a substantial portion of RelA is trapped by the IkBsome complex and does not respond to canonical inhibitor of kappaB kinase (IKK) activation.[41] However, in response to the host cytokine TNF-α, RelA showed a higher amplitude than c-Rel. This may reflect an insufficient response by the c-Rel-binding inhibitor of kappaB (IκB)ε to the transient kinase activity of IKK that is induced by TNF-α.[27,42] For all the ligands, the time to peak of c-Rel was longer in comparison to RelA, which is related to the slope of the first rise of RelA being always greater than that of c-Rel. The other quantitative features (e.g., AUC, attenuation rate) showed ligand-specific differences between the two subunits, which suggests that these signaling features can encode some ligand-specific information (Figure 2B). A correlation analysis showed that some signaling features of RelA and c-Rel were

correlated in spite of non-negligible outliers (e.g., in peak amplitude and duration), which is expected from the shared upstream activation via IKK.[43] However, other signaling features had low correlations (e.g., slope of first rise and attenuation rate) (Figure S2), raising the possibility of additional information content in c-Rel signaling that macrophages could exploit.

The correlation of signaling features between RelA and c-Rel depends on the activating ligand

Having found that non-redundant c-Rel signaling dynamics may transmit additional information for encoding the identity of the activating ligands, we wondered what features of c-Rel signaling might be relevant. To address this question, we dissected the quantitative relationships of RelA and c-Rel signaling in more depth. Taking advantage of the co-signaling data from the same single cells, we calculated the correlation coefficients between RelA and c-Rel signaling features for each ligand time series dataset. The correlations observed within each ligand time series dataset differed from their general correlations found across all the ligand stimulation datasets, termed "pan-ligand" correlations (Figures 2C and S2). For example, the time to peak and duration of the lipopolysaccharide (LPS) time series dataset no longer showed a strong correlation between RelA and c-Rel. The duration of RelA and c-Rel also had a much lower correlation for R848 and CpG compared to the overall pan-ligand correlation across all the ligands.

Cross-correlations of signaling features reveal the sources of RelA and c-Rel divergence in encoding the ligand specificity

The previous result led us to expand and calculate the correlation coefficients for all possible pairs of individual RelA and c-Rel signaling features, which can be displayed in a "correlation matrix" for each dataset. The correlation matrix is thus an exhaustive overview of inter-relationships between signaling features, computed from interrogating the single-cell time series dataset, for a quick identification of signaling features that tend to be linked to each other and those which appear to behave independently. Using the total dataset for all seven ligands, we constructed a pan-ligand correlation matrix (Figure 3A). The panligand correlation matrix represents the generic behavior of RelA and c-Rel signaling features that is not specific to any ligands. This was to serve as a baseline for the ligand-selective correlation matrices that were computed separately using the dataset for each ligand (Figure 3B).

In the pan-ligand correlation matrix, the peak amplitudes of RelA and c-Rel were highly correlated (0.78; Figure 3A), which means that high RelA peaks were followed by high c-Rel peaks in individual cells (RelA nuclear translocation was always faster than c-Rel; Figures 2B and S2). Moreover, within the cross-correlation rectangle of the pan-ligand matrix, several diagonal values (relating the same quantitative features for the two subunits) were generally high. This probably reflects the extent of a shared upstream IKK signaling cascade affecting both NF-κB subunits.[38,44] Some values off the diagonal were interesting, including the strong correlation (0.68) between the peak amplitude of c-Rel and the AUC of RelA. Along this vein, the attenuation rate of RelA was lower (which promotes a

more sustained RelA signaling) when the c-Rel amplitude or AUC was higher (negative correlations −0.36 and −0.35; Figure 3A).

The correlation matrices generated from individual ligand datasets showed interesting deviations from the pan-ligand matrix. We found that the ligand-specific correlation coefficients (diverging by at least 0.45 in absolute values from the pan-ligand counterparts) have remarkably distinct occurrence patterns across the ligands (Figure 3B, marked with green boxes). For example, the time to peak and the duration of RelA and c-Rel signaling are strongly correlated in general (Figure 3A) but much less so in LPS-induced dynamics (Figure 3B, LPS matrix, green boxes). The durations of RelA and c-Rel signaling were even less correlated in the CpG single-cell co-imaging data. For Pam3CSK4, the c-Rel duration was no longer negatively correlated to the number of RelA cycles, in contrast to the panligand. Unlike PAMPs, TNF-α data produced a correlation matrix with only weak cross-correlations between RelA and c-Rel features (Figure 3B, TNF-α matrix). The amplitude of the first c-Rel peak had no effect on the AUC of RelA signaling for TNF-α, whereas they were correlated for most PAMPs (Figure 3B, TNF-α matrix, green boxes, compared to their counterparts in other matrices).

Interestingly, these analyses identified two outlier ligands with opposite properties among the PAMPs. Flagellin, a bacterial PAMP sensed by the TLR5/Myd88 on the cell surface, had the largest number of deviations in the correlation matrix from the pan-ligand (Figure 3B, flagellin matrix, green boxes). On the other hand, poly(I:C), a viral PAMP sensed by TLR3/TRIF in the endosome, is the only ligand with no large deviations in its correlation matrix from the pan-ligand matrix, which suggests that NF-κB signaling dynamics induced by this ligand embody the generic pan-ligand pattern of RelA and c-Rel relations.

A close look at the matrices also indicated that the duration of c-Rel is often involved in the ligand-specific divergence from the pan-ligand correlation matrix (Figure 3B, green boxes in the matrices of LPS, flagellin, CpG, R848, and Pam3CSK). These relations of c-Rel with RelA signaling features are gained, lost, or even switched between positive and negative correlations for different ligands. For example, flagellin had three correlations involving the duration of c-Rel reversed from the pan-ligand (Figure 3B, flagellin matrix, green boxes in a horizontal row from "c-Rel duration" on the y axis, compared to their counterparts in Figure 3A). Altogether, the duration of c-Rel had a great impact on shaping the ligand-specific cross-correlation of RelA and c-Rel signaling features, which will be important later in ligand prediction accuracy of machine learning (ML) models (Table S1).

Ligand discrimination is more precise with signaling features of RelA and c-Rel in comparison to either subunit alone

It was recently shown that distinct signaling codons (similar to the eight quantitative features introduced above) of RelA carry the relevant information to help macrophages distinguish the stimulating ligands.[7] Following the observation that some features of c-Rel signaling dynamics are different from those of RelA, we asked whether c-Rel may relay additional stimulus information to the nucleus. To evaluate the degree of ligand discrimination systematically, we developed supervised ML models by training them with signaling features of RelA, with those of c-Rel, or with those of both RelA and c-Rel, from

the 7-ligand dataset (Figure 4A). Despite some mild correlations between these features, they capture largely independent aspects of signaling dynamics unfolding from early to late phases, like the previously defined signaling codons (Figure S3).[7]

We used two different classification algorithms, K-nearest neighbor (KNN) and linear discriminant analysis (LDA), for learning the ligand-discriminating features. KNN and LDA were chosen to harness their widely complementary advantages and limitations. KNN can handle flexible data distributions with no parametric assumptions (Figure S4), whereas LDA is less prone to overfitting the training data. Their performances in predicting the identity of the activating ligand were assessed in a repeated 10-fold cross-validation: the ML models were trained on randomly sampled 70% of the total dataset and tested on the remaining 30% for model performance in ten independent sampling rounds. To visualize the performance outcome of the multi-class ML predictions, we computed the F1 score, a harmonic mean of the precision and recall, which is an ML performance measure for both balanced and imbalanced datasets (Figure 4B). We also generated the confusion matrix for each ML algorithm that summarizes the predictions made on the test datasets (Figures 4C and S5).

KNN models were more accurate in identifying most ligands (5 out of 7) if the signaling features of both subunits were used for ligand identification (Figures 4 and S5). For example, ML with RelA features alone produced the highest confusion in identifying CpG (only 59% correct on average), with 24% and 13% misclassified as poly(I:C) and Pam3CSK4, respectively. By including c-Rel features, the KNN ML improved the CpG prediction accuracy to 62% by reducing the confusion with Pam3CSK4 to 7%. Notably, signaling features of c-Rel alone were more error prone, but their inclusion resulted in modest improvements of prediction accuracy over ML predictions based on RelA features alone (Figure 4C). Both the c-Rel features that were correlated with RelA and those that were divergent from RelA contributed to the modest improvements (Figure S6). The improvements of prediction accuracy were also observed when the trained ML models were tested on an independent dataset (Figure S7). While the performances of the LDA models were slightly lower than the KNN models (for all ligands except for LPS and TNF-α), the use of both RelA and c-Rel signaling features again improved ligand prediction for most ligands (6 out of 7) (Figure S5). The top two features contributing to the enhanced LDA prediction were the attenuation rate of RelA and the duration of c-Rel (Table S1). Calculation of additional performance measures indicated that the ligand prediction improved mainly through gains in precision and sensitivity for the ML models (Figure S5). These results demonstrate that the signaling dynamics of both NF-κB subunits encode more ligand-discriminating information in comparison to RelA or c-Rel alone.

Signaling features of c-Rel help maintain ligand discrimination at high doses

Since the above data were obtained from ligand stimulations at fixed concentrations, we asked whether different doses affect ligand discrimination. For example, it is conceivable to suspect that some ligands may be hard to distinguish at saturating concentrations when they converge on shared downstream components. To address this, we focused on varying the doses of LPS and TNF-α. First, the time series data indicate that the reference concentrations used above (10 ng/mL for both ligands) are not saturating, as higher doses

produced distinct, often stronger responses in some cells (Figure S8). Moreover, the ML analysis with 10-fold cross-validation within a given dose dataset showed that signaling features of both subunits help maintain the discrimination between the two ligands at high ligand doses better than those of RelA alone (Figure 5A).

Another interesting question that could be addressed with the dose titration data was whether the signaling features learned from a particular dose can predict the ligand identity of time series from unseen doses. To assess cross-dose predictability, ML models were trained on each dataset for a given dose, and then models were tested against the remaining dataset for all the other doses (e.g., training on 1 ng/mL and testing against 10, 100, and 500 ng/mL, and so on). Due to the mismatch of the doses in model training and testing, the prediction accuracy was reduced from the same-dose predictions (Figure 5B). However, ML models performed better if signaling features of both RelA and c-Rel were used, especially for KNN, where the cross-dose prediction accuracy was nearly as high as the same-dose accuracy. These results suggest that macrophages achieve a more robust ligand discrimination over a wide dose range through the signaling features of both RelA and c-Rel.

Mathematical modeling suggests key roles of IκBε in c-Rel-specific encoding of ligand information

Next, we sought to understand the observed single-cell signaling time series data with a mechanistic dynamical systems model. Our rationale for mathematical modeling was 2-fold: first, the RelA and c-Rel co-imaging data for the multiple ligands allowed an opportunity to construct and test a model that merges a previous model of receptor-proximal signaling events[7] with another model of RelA, c-Rel, and their interactions with IκBα and IκBε.[45] The receptor-proximal signaling model[7] included receptor modules for five of the ligands considered here but not for flagellin and R848.

Second, the dual NF-κB dimer macrophage model may then be used to gain further insight into which biochemical reactions are important for the observed relationship between RelA and c-Rel signaling dynamics. We combined the two mathematical models (Figure 6A) by adopting the reaction rates involving RelA and IκBα interactions from the core module of Adelaja et al.[7] and setting the reaction rates involving c-Rel and IκBε to maintain the relative difference between RelA vs. c-Rel and IκBα vs. IκBε as determined by Alves et al.[45] We then tuned a minimum set of parameters from the upstream receptor modules (CD14-LPS association; TLR4 recycling; CpG internalization rate; degradation of TLR1/2, TLR3, and TLR9; synthesis of TLR1/2; TNF-α degradation; and complexed TNF receptor activation) that were not defined by prior biochemical studies, such that fits to the DKI macrophage imaging data could be optimized. As a result, the simulated time courses recapitulated key features of the experimental data (Figure 6B). Quantitative features like peak amplitude and AUC (total activity) demonstrate a reasonable match between experimental and model trajectories (Figure 6C). The cross-correlation analysis highlighted the duration of c-Rel as a recurrent signaling feature whose relationship with RelA features (e.g., AUC or duration) exhibits ligand specificity. Since it is experimentally intractable to

modulate dynamic features of c-Rel precisely, we opted for a theoretical exposition with our data-constrained mathematical model and performed *in silico* manipulations.

To interrogate the role of parameters that regulate the dynamical characteristics of RelA and c-Rel response trajectories, we devised a computational workflow focusing on interactions that contained significant differences between the NF-κB and IκB isoforms (Figure 6D; STAR Methods). This workflow begins with sampling parameters for the association and dissociation rate constants between NF-κBs and IκBs and between IKK and IκBs within ranges that encompassed the values of each isoform and would explore their sensitivity. The effective IκB-NF-κB Kd values were varied between 3.2×10^{-7} and 2.9×10^{-3} μM and IKK-IκB Kd values were varied between 0.1 and 1.6 μM. The resulting activation trajectories of RelA and c-Rel in response to TNF-α and LPS were simulated for each sampled parameter set. The trajectories were then decomposed into the signaling codons, which were then used as the basis for clustering and dimensionality reduction (Figure 6D). We identified 6 clusters in the high dimensional space and projected it onto a two-dimensional principal-component analysis graph, which captured just over 50% of the variance in the data (Figure 6E). Cluster means showed distinct paired RelA and c-Rel trajectories, revealing differences not only in the degree of activation and oscillations but also in the differences between RelA and c-Rel dynamics (Figure 6E). We then painted the values of specific parameters on this landscape of RelA and c-Rel signaling dynamics (Figure 6F). For example, we observed a region (around clusters 2 and 3) where c-Rel activation in response to TNF-α exceeds that of RelA because of abnormally high values (poor affinity) in the IκBα-c-Rel Kd and IKK-IκBα Kd. In contrast, we observe a region (around clusters 1 and 5, containing the wild-type [WT] parameter set) where RelA activation in response to TNF-α exceeds that of c-Rel, where the values of IκBε-RelA Kd and IKK-IκBε Kd are high. Importantly, many alternative parameter sets resulted in less distinction between RelA and c-Rel signaling dynamics, supporting the hypothesis that the differences in interaction affinities of RelA and c-Rel for IκBα and IκBε, and differences in stimulus-responsive degradation rates of IκBα and IκBε mediated by IKK, are critical for the observed differential dynamics of these two NF-κB family members.

RelA and c-Rel dynamics from IκBα and IκBε mutant macrophages agree with model predictions

To further interrogate the mathematical model, we developed simulations for RelA and c-Rel response dynamics in virtual genetic mutants that could be tested experimentally. The first, IκBε KO, is a complete KO of IκBε, as described previously.[27] The second, the IκBα mutant, harbors mutated κB sites in the IκBα promoter, making it defective in NF-κB-induced expression of IκBα.[46] The translation rate of the IκBε transcript was set to zero to model the IκBε KO, and the maximum RelA-induced transcription rate of IκBα was reduced 4-fold to model the IκBα mutant to match the published IκBα expression time course. Model simulations predicted significant changes to NF-κB dynamics in response to TNF-α in these mutants, while changes in response to LPS were more subtle (Figure 7A). In the IκBε KO, loss of IκBε results in increased TNF-α-response activity of c-Rel, as exemplified by peak amplitude. Furthermore, the response was more oscillatory. However,

in the IκBα mutant model, the simulated TNF-α responses were less oscillatory, with little change in the amplitude.

To test these predictions, we took advantage of *IκBε*[−/−27] and IκBα[m/m46] mouse strains and bred them into another fluorescence fusion-protein reporter strain for RelA and c-Rel as well as the nuclear reporter mCherry-H2B strain. These NF-κB reporter mouse strains contained different fluorescent proteins, the mice were maintained at a different institution, and the experimental data were produced using different instrumentation and slightly different protocols. Focusing on the comparison between mutants and the matching WT reporter, we found that RelA and c-Rel trajectories in response to TNF-α were elevated in the IκBε KO, while responses to LPS were much less affected (Figures 7B and S9), matching model predictions. For example, the peak amplitude of RelA and c-Rel trajectories for TNF-α was slightly higher in the IκBε KO (Figure 7C). Furthermore, oscillatory features were persistent and clearly identifiable in RelA trajectories from the IκBε KO, consistent with prior studies.[27,47,48] In the IκBα mutant, oscillatory power was reduced in RelA trajectories in response to TNF-α, as seen previously.[7] Finally, responses were faster when cells rely on IκBα in the absence of IκBε, as evidenced by the shorter time to first peak in the IκBε KO. These findings confirm the mathematical model's prediction that the biochemical characteristics of IκBε reduce the NF-κB response to TNF-α, thereby providing an explanation for why c-Rel, with its higher affinity for IκBε, is relatively unresponsive to TNF-α.

Although it is experimentally intractable to modulate biochemical interaction constants directly to test this plausible explanation further, we opted for a theoretical exposition with our data-constrained mathematical model and performed *in silico* manipulations. Specifically, we modified two key reactions involving IκBε, given their roles in shaping c-Rel dynamics in B cells.[45] First, we changed the higher affinity of IκBε for c-Rel to the same as that for RelA by setting the dissociation rate constant for IκBε and RelA binding to be the same as that for IκBε and c-Rel. Next, since IκBε is set to have a lower sensitivity to IKK-induced degradation in the model,[45,49] we also examined the effect of making the IKK-mediated IκBε degradation rate equal to the corresponding rate for IκBα. The model simulations for both scenarios confirmed that these reactions are control points for c-Rel duration, but they also affected other features such as peak amplitude and the extent of oscillations (Figure 7D). Importantly, the altered parameters resulted in less distinction between RelA and c-Rel dynamics than observed in the WT data, supporting the hypothesis that the differences in interaction affinities of RelA and c-Rel for IκBα and IκBε and the differences in stimulus-induced degradation rates of IKK-mediated IκBα and IκBε are critical for the observed differential dynamics of these two NF-κB family members.

DISCUSSION

Here, we examined dynamic characteristics of the NF-κB subunit c-Rel simultaneously with the widely considered subunit RelA in the same cells by live imaging, with unprecedented quantitative detail using an endogenous DKI mouse line. Co-imaging RelA and c-Rel was possible through the availability of the fluorescent c-Rel endogenous KI mice[39] that put c-Rel on par with the other transactivating subunits, RelA and RelB, of NF-κB.[50,51] Our

results reveal the dynamic features, or signaling codons, of c-Rel that are linked to the nature of the activating PAMP and distinct from those of RelA. This supports previous studies that suggest distinct functions of c-Rel[36,52] and further challenges the idea that c-Rel is another canonical subunit with redundant patterns of signaling dynamics as RelA (Figure 8). We focused on macrophages, an immune sentinel cell type, but a similar approach may shed light on the impact of c-Rel in other immune cell types as well.

The two subunits differed from the earliest signaling event following NF-κB activation, the nuclear translocation. Our co-imaging of DKI macrophages allowed an accurate, controlled comparison of the nuclear translocation rates for RelA and c-Rel. The accumulation of RelA in the nucleus reached a peak faster than c-Rel, for all the activating ligands without exception, as quantified by two signaling features (shorter time to peak and higher slope of the first rise for RelA vs. c-Rel). This likely reflects its control by IκBα, which is more responsive to IKK, in comparison to IκBε. This pattern has a noteworthy consequence at NF-κB target chromatin, giving RelA a competitive advantage over c-Rel for interacting with the regulatory sites in the epigenome. Depending on the genomic context and the nature of RelA interactions, the κB-motif-containing locus may be unavailable for regulatory actions of c-Rel if RelA occupancy is long lived. In other sites where RelA binding may be short lived, early occupancy of RelA may potentially prime the sites for subsequent c-Rel action. These possibilities indicate how previous data on c-Rel effects may be re-interpreted and also raise new questions about how RelA and c-Rel might regulate the induction of immediate-early genes through potential competition or coordination at target chromatin sites.

Although it is thought that both combinatorial and dynamic signaling may underlie the specificity of macrophage responses to various PAMPs,[53] it remains difficult to quantify their relative contributions in individual primary immune cells. In this regard, it is quite remarkable that ML models trained on NF-κB dynamics alone have rather high ligand prediction accuracies (62%–95% with KNN models using RelA and c-Rel features), given the other factors such as AP-1 and IRFs that are also activated downstream of TLRs. It is possible that the other factors may further improve the ligand discrimination capability to even higher precision, or they may reinforce the information encoding of NF-κB against noisy single-cell behaviors. Here, we focused on how much of the ligand information is encoded by RelA and c-Rel dynamics. Future studies should also examine the functional consequence of the information content and the gain enabled by c-Rel in terms of gene regulation since RelA and c-Rel have different promoter binding specificities[36,54] and can interact with co-activators differently.[55–57] Immunologically relevant cell types and endogenous target genes within a well-characterized genomic regulatory landscape would be particularly interesting to examine with an approach combining quantitative live-cell imaging and genomic assays, where the relationship between NF-κB signaling and gene regulation can be discerned.[13,18,58]

Our in-depth analysis uncovered that the ligand-discriminating information is engrained partly in the way in which c-Rel signaling duration is related to the signaling features of RelA in macrophage responses to the activating ligands. The analysis also revealed poly(I:C) as a generic PAMP exemplifying the consensus macrophage NF-κB signaling,

while flagellin emerged as a "specialty" ligand with a unique signaling pattern. We noted that poly(I:C) is likely the most evolutionarily ancient signal since its receptor TLR3 is the most conserved TLR subfamily of genes among vertebrates.[59] On the other hand, flagellin may be a relatively recent PAMP that the host has evolved to deal with, as evidenced by the positive selection for its receptor TLR5 in vertebrate evolution.[59] The coordinated vs. independent aspects of RelA and c-Rel signaling that support macrophage ligand discrimination may have emerged from the host immune responses against the changing pathogen landscape during evolution.

Limitations of the study

The functional relevance of the additional information encoded by c-Rel signaling features needs further investigation. It is technically challenging to address this since such studies require a perturbation that alters specific features of c-Rel signaling or macrophage-specific inducible KO of c-Rel, which is out of scope of this study.

Mathematical modeling was focused on the roles of IκBα and IκBε in the IKK-NF-κB signaling network based on previous studies. However, we cannot rule out other mechanisms that may underlie the distinct features of RelA and c-Rel signaling dynamics.

The IκBα mutant and IkBe KO experiments (along with WT controls) were performed on a different reporter mouse strain at different technical settings (institution, vivarium, BMDM differentiation protocol, microscope, optical properties of fluorescent reporter proteins such as photobleaching and spectral overlaps, image acquisition parameters, image quantification and analysis). While a direct comparison of NF-κB dynamic patterns in the WT BMDMs from the two reporter systems is complicated by the different experimental setups, it is significant that the key conclusions about the differential dynamics of RelA vs. c-Rel in response to TNF-α and LPS are reproduced.

STAR★METHODS

RESOURCE AVAILABILITY

Lead contact—Further information and requests for resources and reagents should be directed to the Lead Contact, Myong-Hee Sung (sungm@nih.gov).

Materials availability—The NF-κB double knock-in reporter mice were previously described[39] and are available upon completion of a Material Transfer Agreement according to the NIH guidelines. mTFP1-cRel, mVenus-RelA, IκBα-mut mice are available from the Jackson Laboratory. mCherry-H2B mice are available from the RIKEN BioResource Center. Nfkbie KO mice are available upon completion of an MTA with UCLA. No unique reagents were generated in this study.

Data and code availability

- All the time series replicate data have been deposited and are available at https://github.com/Toufiq54/Ligand-Discrimination-from-RelA-and-c-Rel-signaling-dynamics-in-primary-macrophages.

- All the original code for image quantification and analysis have been deposited and are available at https://github.com/Toufiq54/Ligand-Discrimination-from-RelA-and-c-Rel-signaling-dynamics-in-primary-macrophages. All code for NF-κB mathematical modeling and simulations is available at https://github.com/apekshasingh/Rela_cRel_Model.

- Any additional information required to reanalyze the data reported in this paper is available from the lead contact upon request.

EXPERIMENTAL MODEL AND STUDY PARTICIPANT DETAILS

Mice—The mEGFP-RelA mScarlet-*c*-Rel double knock-in (DKI) mice were described previously.[39] These mice have mEGFP and mScarlet knocked into the transcription start sites of Rela and Rel, respectively, producing N-terminal fusion proteins of each from the endogenous loci. All animals were bred and maintained under specific pathogen-free conditions at the animal facility of National Institute on Aging. All the animal care and procedures in this study were carried out in accordance with the guidelines of NIH and approved by the NIA Animal Care and Use Committee. 9–11 week old male mice homozygous for both knock-in reporters were used for experiments.

Triple reporter mVenus-RelA, mTFP-cRel, mCherry-H2B mice[60](Narayanan et al., in revision) were crossed into an $I\kappa B\epsilon^{-/-}$ line[27] and a strain harboring mutated κB sites in the IκBα promoter.[46] The experimental mice were 6–12 weeks of age with the genotype cRel $^{mTFP1/mTFP1}$, RelA$^{mVenus/mVenus}$, and H2B$^{mCherry/+}$, and either WT, $I\kappa B\epsilon^{-/-}$, or $I\kappa B\epsilon^{mut/mut}$. Mice were housed and handled according to guidelines established by the UCLA Animal Research Committee under an approved protocol.

Primary BMDM culture—Bone marrow-derived macrophages (BMDMs) were obtained by culturing the bone marrow cells from femurs and tibia of homozygous green-red DKI mice (9–12 weeks age) in M-CSF containing media for 6 days. BMDMs were re-plated in a fibronectin-coated glass-bottom μ-Slide 8-well high (ibidi) on day 6. The coated glass-bottom surface was prepared by incubating 5 μg/cm^2 plasma fibronectin (Fisher Scientific, cat# FC010) for 1 h at 37°C. The next day, BMDMs were stimulated with one of the following ligands: 10 ng/mL lipopolysaccharide (LPS, Enzo Life Science, #ALX-581-008-L001), 250 ng/mL Flagellin (ThermoFisher Scientific, #C905R23), 25 μg/mL of CpG (InvivoGen, #tlrl-2395), 20 μg/mL of Poly(I:C) (InvivoGen, # tlrl-picw), 350 ng/mL of R848 (InvivoGen, #tlrl-r848), 40 ng/mL of Pam3CSK4 (InvivoGen, # tlrl-pms), 10 ng/mL of murine TNF-α (R&D Systems, Cat#410-MT-010).

For the IκBα mutant and IkBe knockout experiments (with wild-type controls), BMDMs were obtained by culturing bone marrow cells from the femurs and tibia of reporter mice (6–12 weeks age) in L929 supplemented media. On day 4, BMDMs were re-plated into 8-well μ-slides (Ibidi, #80826) at 25000–30000 cells/cm^2. Cells were stimulated on Day 7 or 8 with 10 ng/ml LPS (Sigma-Aldrich, #L6529-1MG) or 10 ng/ml TNF (R&D Systems, #410-MT-0101).

METHOD DETAILS

Live-cell microscopy—Primary cells from NF-κB green-red double knock-in reporter mice were plated in a fibronectin-coated glass-bottom μ-Slide 8-well high imaging chamber (ibidi, Cat# 80806) and cultured for 24 h in phenol red free DMEM (Gibco, Cat# 21063029) supplemented with 10% FBS, 1% penicillin, streptomycin, and glutamine. Cells were stained with SPY650-DNA dye (1x or 1.5x of recommended dilution, molarity not indicated by manufacturer) 1 h before the live-cell imaging experiment. The high-throughput, high-resolution, and multi-channel live-cell imaging of lowly abundant endogenous proteins was carried out in Zeiss LSM 880 with Airyscan detector system and with 40× oil objective. The glass surface of 8-well imaging slide was pre-wetted with the immersion oil for long-term fluorescent microscopy with oil objective without drying out the contact between the bottom glass-surface and oil-objective. Cells were then placed in a Zeiss LSM880 Airyscan AxioObserver confocal microscope system with incubation, and were maintained at 37°C in a humidified environment containing 5% CO_2. Cells were incubated about 1~2 h before the live-cell imaging experiment started. Time-lapse images were acquired at 7-min intervals for a time-course of ~12.5 h (150 frames). Excitation laser wavelengths were 488 for EGFP, 561 nm for mScarlet, and 633 nm for SPY650-DNA dye. Fluorescence signals were detected using the Airyscan detector. Imaging parameters were: a 40x/1.4 NA Plan-Apochromat oil objective, pinhole size 5.16 AU, 4.60 AU, and 4.07 AU for mEGFP, mScarlet, and SPY650-DNA, respectively. Frame scan mode, 0.6 scan zoom, 2.06 μs pixel time, line time 30.00 μs, frame time 1.90 s, unidirectional scan direction, 12 bit, 512×512 image size. The detector and digital gains are 960.5, 850.0, 760.0 and 1.0, 1.4, 1.2 for mEGFP, mScarlet, and SPY650-DNA, respectively. Images were saved in .czi file and later converted to .tiff for further analysis.

For the IκBα mutant and IκBε knockout experiment, cells were placed on a Zeiss Axio Observer.Z1 inverted microscope with live-cell incubation and maintained in the 37°C humidified environment containing 5% CO_2 for at least 60 min to equilibrate. Time-lapse images were acquired at 5-min intervals using a Plan-Apochromat 20x/0.8NA M27 air objective for a time course of 12 h. Images were collected sequentially in four channels, mCherry (filter set Semrock mCherry, excitation 542-582nm, beam splitter: 593nm, emission 604-678nm, Colibri.2 30%, exposure 200ms), mVenus (filter set Zeiss 46 HE, excitation 488-512nm, beam splitter 515nm, emission 520-550nm, Colibri.2 80%, exposure 160ms), mTFP (filter set Zeiss 47 HE, excitation 424-448nm, beam splitter: 455nm, emission 460-500nm, Colibri.2 80%, exposure 950ms), and for differential interference contrast (DIC) (HAL 100 lamp, 2.5V, exposure: 20ms). Images were recorded on a Hamahatsu Orca Flash4.0 CMOS camera with 2x2 binning. After collection of baseline images for 1 h, the indicated stimulus diluted in conditioned media was applied using syringe injection into the chamber *in situ* and images were acquired for an additional 12 h.

QUANTIFICATION AND STATISTICAL ANALYSIS

Quantitative analysis of time lapse imaging data—The live-cell microscopy images were analyzed to obtain the single-cell signaling measurements using custom-written MATLAB script (MATLAB 2020b). In brief, acquired.czi files were first converted to.tif files for all positions and channels. The nuclear area of individual cells was segmented

using the SPY650-DNA nuclear dye channel images. The cellular area was segmented using either the mEGFP or the mScarlet channel. Segmented cells were tracked across successive images using the lineage mapper tracking tool.[61] Then, nuclear, cytosolic, and total fluorescence intensities were calculated from the background-subtracted images for both mEGFP and mScarlet channels. The cells coming in or going out from the field of view, along with apoptotic or dividing cells, were excluded from the analysis. The analysis codes are available upon request.

For the IκBα mutant and IκBε knockout experiments, the single cells were segmented into cytoplasm and nucleus using the mCherry nuclear signal and tracked across the 12-h time course. The basal nuclear presence was determined from 12 time points prior to stimulation. Basal nuclear activity was subtracted from subsequent measurements. When measurements fall below the basal level, negative values were reported. A ratio of nuclear over total fluorescence was quantified using mean nuclear fluorescence and cytosolic mean fluorescence. The cytoplasm was represented by an annulus around the nucleus using a nuclear to cytoplasmic ratio of 1:3.5. The fluorescence was quantified using MACKtrack in MATLAB 2015a (Adelaja et al., 2021 available at github.com/signalingsystemslab/MACKtrack).

Machine learning (ML) analysis—Based on the recently introduced signaling codons[7] and other related dynamic features,[24,39,40] we had selected eight features to encompass all possible signaling dynamics of RelA and c-Rel. We had also refined the definitions to minimize artifactual values called by the analysis algorithm. We reasoned that the data-driven relationships will emerge from the more accurate quantification of dynamic features. The eight signaling features of single-cell RelA and c-Rel trajectories were extracted using custom-written MATLAB scripts. The signaling features were imported into the R-programming language environment for ML analysis. 70% of each ligand dataset were randomly sampled for training purposes and the rest 30% were used for testing the model. The random sampling was repeated for a 10-fold cross-validation of each trained model in all the analyses. Two different ML algorithms were used to train the models: a. k-nearest neighbors (KNN), and b. linear discriminant analysis (LDA). The models were trained with either the RelA signaling features, the c-Rel signaling features, or the signaling features of both RelA and c-Rel. We utilized the R-packages MASS and caret for LDA analysis and KernelKnn for generating the KNN models. For KernelKnn, the Canberra distance metric and K = 7 were used in all the KNN analyses, because these options produced the best performance in an extensive comparison of all the available metrics and K values. The performance measures depended more on the distance metric than on the choice of K. While the F1 score and sensitivity showed K = 5 being equally good, we chose K = 7 because of the slight increase in accuracy and precision (Figure S4). The stepLDA function of the caret package was used to select the important features of LDA models. The ML analysis plots were generated using MATLAB scripts. The codes for ML analysis and plotting are available upon request.

Mathematical modeling

Model topology: A model for simulating the dynamics of NF-κB dimers RelA:p50 and c-Rel:p50 (below referred to as RelA and c-Rel for brevity) in response to the seven ligands used in the described experiments was constructed by combining and extending two previously published models. A model that recapitulates RelA NF-κB dynamics of BMDMs in response to TNFR1, TLR1/2, TLR3, TLR4, TLR9[7] was extended by formulating models for the TLR5 and TLR7/8 signaling modules to account for Flagellin and R848 stimulation datasets, respectively. Flagellin binds to TLR5 at the cell surface and the ligand-receptor complex activates MyD88. R848 is first internalized into endosomes where it binds TLR7/8, and the ligand-receptor complex also activates MyD88.

The core IKK-NF-κB signaling module[7] was extended with interactions involving IκBε and c-Rel as described (Alves et al., 2014). Accordingly, IκBα and IκBε were set to bind and inhibit RelA and c-Rel with different affinities. Terms for IκBα and IκBε synthesis and induced transcription by RelA- and c-Rel-containing NF-κB dimers were based on.[47] Accordingly, nuclear RelA was set to induce the synthesis of IκBα and IκBε, while nuclear c-Rel induced only IκBε synthesis.

The concentrations of all the species containing c-Rel or RelA in the nucleus and cytoplasm obtained from model simulations were used to calculate the ratio of nuclear NF-κB to total NF-κB, to match the ratio of nuclear to total cell intensity of RelA or c-Rel from the experimental data. The experimental ratio was subtracted using the baseline ratio at zero hours, as the model assumed that the cell starts with no nuclear NF-κB at t = 0. The NF-κB ratio was scaled by adding a constant concentration of RelA (0.13 μM) and c-Rel (0.035 μM) to the total NF-κB concentration that is untranslocatable, as it is sequestered by IκB complexes.

Model parameters: For new TLR modules, ligand-receptor dissociation constants were obtained from the literature.[62–64] Other parameters were based on other TLR modules and tuned to recapitulate the experimental data as described below. Parameters for IκBε and c-Rel reactions in the core IKK-NF-κB module were based on previously determined ratios to IκBα and RelA reactions.[45] Basal synthesis of IκBε was adjusted to reflect lower expression in macrophages compared to B-cells.

Model parameters in the TLR/TNFR modules were tuned to improve the visual fit. The model was run for 12 h for all ligands, with a priority for fitting early activity. PAM3CSK4 signaling was delayed by 90 min to fit the initial peak of the single-cell data. Subsequent fitting of NF-κB dynamics for each of the seven ligands was achieved through tuning upstream TLR/TNFR module parameters within a 10-fold range, while minimizing the number of varied parameters ("multi-stimulus NFkB.xlsx" in Github repository: Rela_cRel_Model/Model_Script). As a result, parameters for the following reactions were altered: TNF degradation and activation of complexed TNFR, CD14-LPS association and TLR4 recycling, the CpG internalization rate and the degradation of bound TLR9, degradation of free and bound TLR3, TLR1/2 synthesis and the degradation of bound receptor.

Parameter variation: To interrogate parameter value sensitivity to model interpretation, the IκB-NF-κB Kd values were varied between 3.2e-7 and 2.9e-3 μM and IKK-IκB Kd parameter values were varied between 0.1 and 1.6 μM. The Kd parameter ranges were chosen to encompass the values of the isoforms, including the dissociation rate constants of IκBα-RelA, IκBα-*c*-Rel, IκBε-RelA, IκBε-*c*-Rel, and the association rate constants of IKK-IκBα and IKK-IκBε. Parameter values were sampled 100,000 times and model simulations in response to TNF-α and LPS stimulation were collected. The 100,000 simulated trajectories were decomposed into four signaling codons, including peak amplitude, time to peak, total integral (AUC), and number of peaks. Hence each parameter set was associated with 16 feature values (TNF-α or LPS (2) x RelA or c-Rel (2) x trajectory features (4)). The difference between RelA and c-Rel features were used for K-means clustering into 6 groups and dimensionality reduction via Principal Component Analysis (PCA) (MATLAB version R2019b).

To model the IκBε KO,[27,47] the IκBε translation rate constant was set to zero. To model the IκBα mutant in which several κB sites in the IκBα promoter are mutated,[46] the V_{max} of RelA-induced transcription of IκBα was reduced by 4-fold. Additional parameter variations were explored with the model to assess differences between c-Rel and RelA dynamics not accessible through experimental perturbations: 1) setting the K_d of IκBε-RelA interaction to that of IκBε-*c*-Rel and 2) setting the K_d of IKK-IκBε binding to that of IKK-IκBα.

Supplementary Material

Refer to Web version on PubMed Central for supplementary material.

ACKNOWLEDGMENTS

REFERENCES

1. Levchenko A, and Nemenman I (2014). Cellular noise and information transmission. Curr. Opin. Biotechnol 28, 156–164. 10.1016/j.copbio.2014.05.002. [PubMed: 24922112]

2. Cheong R, Rhee A, Wang CJ, Nemenman I, and Levchenko A (2011). Information transduction capacity of noisy biochemical signaling networks. Science 334, 354–358. 10.1126/science.1204553. [PubMed: 21921160]

3. Rand U, Rinas M, Schwerk J, Nöhren G, Linnes M, Kröger A, Flossdorf M, Kály-Kullai K, Hauser H, Höfer T, and Köster M (2012). Multilayered stochasticity and paracrine signal propagation shape the type-I interferon response. Mol. Syst. Biol 8, 584. 10.1038/msb.2012.17. [PubMed: 22617958]

4. Hannanta-Anan P, and Chow BY (2016). Optogenetic Control of Calcium Oscillation Waveform Defines NFAT as an Integrator of Calcium Load. Cell Syst. 2, 283–288. 10.1016/j.cels.2016.03.010. [PubMed: 27135540]

5. Selimkhanov J, Taylor B, Yao J, Pilko A, Albeck J, Hoffmann A, Tsimring L, and Wollman R (2014). Systems biology. Accurate information transmission through dynamic biochemical signaling networks. Science 346, 1370–1373. 10.1126/science.1254933. [PubMed: 25504722]

6. Tang Y, Adelaja A, Ye FXF, Deeds E, Wollman R, and Hoffmann A (2021). Quantifying information accumulation encoded in the dynamics of biochemical signaling. Nat. Commun 12, 1272. 10.1038/s41467-021-21562-0. [PubMed: 33627672]

7. Adelaja A, Taylor B, Sheu KM, Liu Y, Luecke S, and Hoffmann A (2021). Six distinct NFkappaB signaling codons convey discrete information to distinguish stimuli and enable appropriate macrophage responses. Immunity 54, 916–930.e7. 10.1016/j.immuni.2021.04.011. [PubMed: 33979588]

8. Li P, and Elowitz MB (2019). Communication codes in developmental signaling pathways. Development 146, dev170977. 10.1242/dev.170977. [PubMed: 31249008]

9. Zambrano S, De Toma I, Piffer A, Bianchi ME, and Agresti A (2016). NF-kappaB oscillations translate into functionally related patterns of gene expression. Elife 5, e09100. 10.7554/eLife.09100. [PubMed: 26765569]

10. Lee REC, Qasaimeh MA, Xia X, Juncker D, and Gaudet S (2016). NF-kappaB signalling and cell fate decisions in response to a short pulse of tumour necrosis factor. Sci. Rep 6, 39519. 10.1038/srep39519. [PubMed: 28004761]

11. Purvis JE, and Lahav G (2013). Encoding and decoding cellular information through signaling dynamics. Cell 152, 945–956. 10.1016/j.cell.2013.02.005. [PubMed: 23452846]

12. Heltberg M, Kellogg RA, Krishna S, Tay S, and Jensen MH (2016). Noise Induces Hopping between NF-kappaB Entrainment Modes. Cell Syst 3, 532–539.e533. 10.1016/j.cels.2016.11.014. [PubMed: 28009264]

13. Aqdas M, and Sung MH (2023). NF-kappaB dynamics in the language of immune cells. Trends Immunol. 44, 32–43. 10.1016/j.it.2022.11.005. [PubMed: 36473794]

14. O'Dea E, and Hoffmann A (2010). The regulatory logic of the NF-kappaB signaling system. Cold Spring Harb. Perspect. Biol 2, a000216. 10.1101/cshperspect.a000216. [PubMed: 20182598]

15. Medzhitov R, and Horng T (2009). Transcriptional control of the inflammatory response. Nat. Rev. Immunol 9,692–703. 10.1038/nri2634. [PubMed: 19859064]

16. Alcamo E, Hacohen N, Schulte LC, Rennert PD, Hynes RO, and Baltimore D (2002). Requirement for the NF-kappaB family member RelA in the development of secondary lymphoid organs. J. Exp. Med 195, 233–244. 10.1084/jem.20011885. [PubMed: 11805150]

17. Kaileh M, and Sen R (2012). NF-kappaB function in B lymphocytes. Immunol. Rev 246, 254–271. 10.1111/j.1600-065X.2012.01106.x. [PubMed: 22435560]

18. Cheng QJ, Ohta S, Sheu KM, Spreafico R, Adelaja A, Taylor B, and Hoffmann A (2021). NF-kappaB dynamics determine the stimulus specificity of epigenomic reprogramming in macrophages. Science 372, 1349–1353. 10.1126/science.abc0269. [PubMed: 34140389]

19. DeFelice MM, Clark HR, Hughey JJ, Maayan I, Kudo T, Gutschow MV, Covert MW, and Regot S (2019). NF-κB signaling dynamics is controlled by a dose-sensing autoregulatory loop. Sci. Signal 12, eaau3568. [PubMed: 31040261]

20. Hughey JJ, Gutschow MV, Bajar BT, and Covert MW (2015). Single-cell variation leads to population invariance in NF-κB signaling dynamics. Mol. Biol. Cell 26, 583–590. [PubMed: 25473117]

21. Lane K, Van Valen D, DeFelice MM, Macklin DN, Kudo T, Jaimovich A, Carr A, Meyer T, Pe'er D, Boutet SC, and Covert MW (2017). Measuring Signaling and RNA-Seq in the Same Cell Links Gene Expression to Dynamic Patterns of NF-kappaB Activation. Cell Syst. 4, 458–469.e455. 10.1016/j.cels.2017.03.010. [PubMed: 28396000]

22. Nelson DE, Ihekwaba AEC, Elliott M, Johnson JR, Gibney CA, Foreman BE, Nelson G, See V, Horton CA, Spiller DG, et al. (2004). Oscillations in NF-kappaB signaling control the dynamics of gene expression. Science 306, 704–708. 10.1126/science.1099962. [PubMed: 15499023]

23. Sung MH, Salvatore L, De Lorenzi R, Indrawan A, Pasparakis M, Hager GL, Bianchi ME, and Agresti A (2009). Sustained oscillations of NF-kappaB produce distinct genome scanning and gene expression profiles. PLoS One 4, e7163. 10.1371/journal.pone.0007163. [PubMed: 19787057]

24. Tay S, Hughey JJ, Lee TK, Lipniacki T, Quake SR, and Covert MW (2010). Single-cell NF-kappaB dynamics reveal digital activation and analogue information processing. Nature 466, 267–271. 10.1038/nature09145. [PubMed: 20581820]

25. Wang AG, Son M, Kenna E, Thom N, and Tay S (2022). NF-κB memory coordinates transcriptional responses to dynamic inflammatory stimuli. Cell Rep. 40, 111159. [PubMed: 35977475]

26. Zhang Q, Gupta S, Schipper DL, Kowalczyk GJ, Mancini AE, Faeder JR, and Lee REC (2017). NF-κB dynamics discriminate between TNF doses in single cells. Cell Syst. 5, 638–645.e5. [PubMed: 29128333]

27. Hoffmann A, Levchenko A, Scott ML, and Baltimore D (2002). The IkappaB-NF-kappaB signaling module: temporal control and selective gene activation. Science 298, 1241–1245. 10.1126/science.1071914. [PubMed: 12424381]

28. Shih VFS, Kearns JD, Basak S, Savinova OV, Ghosh G, and Hoffmann A (2009). Kinetic control of negative feedback regulators of NF-kappaB/RelA determines their pathogen- and cytokine-receptor signaling specificity. Proc. Natl. Acad. Sci. USA 106, 9619–9624. 10.1073/pnas.0812367106. [PubMed: 19487661]

29. Werner SL, Barken D, and Hoffmann A (2005). Stimulus specificity of gene expression programs determined by temporal control of IKK activity. Science 309, 1857–1861. 10.1126/science.1113319. [PubMed: 16166517]

30. Hayden MS, and Ghosh S (2012). NF-kappaB, the first quarter-century: remarkable progress and outstanding questions. Genes Dev. 26, 203–234. 10.1101/gad.183434.111. [PubMed: 22302935]

31. Beg AA, and Baltimore D (1996). An essential role for NF-kappaB in preventing TNF-alpha-induced cell death. Science 274, 782–784. 10.1126/science.274.5288.782. [PubMed: 8864118]

32. Beg AA, Sha WC, Bronson RT, Ghosh S, and Baltimore D (1995). Embryonic lethality and liver degeneration in mice lacking the RelA component of NF-kappa B. Nature 376, 167–170. 10.1038/376167a0. [PubMed: 7603567]

33. Köntgen F, Grumont RJ, Strasser A, Metcalf D, Li R, Tarlinton D, and Gerondakis S (1995). Mice lacking the c-rel proto-oncogene exhibit defects in lymphocyte proliferation, humoral immunity, and interleukin-2 expression. Genes Dev. 9, 1965–1977. 10.1101/gad.9.16.1965. [PubMed: 7649478]

34. Liou HC, and Smith KA (2011). The roles of c-rel and interleukin-2 in tolerance: a molecular explanation of self-nonself discrimination. Immunol. Cell Biol 89, 27–32. 10.1038/icb.2010.120. [PubMed: 20975733]

35. Saibil SD, Jones RG, Deenick EK, Liadis N, Elford AR, Vainberg MG, Baerg H, Woodgett JR, Gerondakis S, and Ohashi PS (2007). CD4+ and CD8+ T cell survival is regulated differentially by protein kinase Ctheta, c-Rel, and protein kinase B. J. Immunol 178, 2932–2939. 10.4049/jimmunol.178.5.2932. [PubMed: 17312138]

36. Sanjabi S, Hoffmann A, Liou HC, Baltimore D, and Smale ST (2000). Selective requirement for c-Rel during IL-12 P40 gene induction in macrophages. Proc. Natl. Acad. Sci. USA 97, 12705–12710. 10.1073/pnas.230436397. [PubMed: 11058167]

37. Hoffmann A, Leung TH, and Baltimore D (2003). Genetic analysis of NF-kappaB/Rel transcription factors defines functional specificities. EMBO J. 22, 5530–5539. 10.1093/emboj/cdg534. [PubMed: 14532125]

38. Fitzgerald KA, and Kagan JC (2020). Toll-like Receptors and the Control of Immunity. Cell 180, 1044–1066. 10.1016/j.cell.2020.02.041. [PubMed: 32164908]

39. Rahman SMT, Aqdas M, Martin EW, Tomassoni Ardori F, Songkiatisak P, Oh KS, Uderhardt S, Yun S, Claybourne QC, McDevitt RA, et al. (2022). Double knockin mice show NF-kappaB trajectories in immune signaling and aging. Cell Rep. 41, 111682. 10.1016/j.celrep.2022.111682. [PubMed: 36417863]

40. Martin EW, Pacholewska A, Patel H, Dashora H, and Sung MH (2020). Integrative analysis suggests cell type-specific decoding of NF-kappaB dynamics. Sci. Signal 13, eaax7195. 10.1126/sci-signal.aax7195. [PubMed: 32098801]

41. Basak S, Kim H, Kearns JD, Tergaonkar V, O'Dea E, Werner SL, Benedict CA, Ware CF, Ghosh G, Verma IM, and Hoffmann A (2007). A fourth IkappaB protein within the NF-kappaB signaling module. Cell 128, 369–381. 10.1016/j.cell.2006.12.033. [PubMed: 17254973]

42. Cheong R, Bergmann A, Werner SL, Regal J, Hoffmann A, and Levchenko A (2006). Transient IkappaB kinase activity mediates temporal NF-kappaB dynamics in response to a wide range of tumor necrosis factor-alpha doses. J. Biol. Chem 281, 2945–2950. 10.1074/jbc.M510085200. [PubMed: 16321974]

43. Cruz JA, Mokashi CS, Kowalczyk GJ, Guo Y, Zhang Q, Gupta S, Schipper DL, Smeal SW, and Lee REC (2021). A variable-gain stochastic pooling motif mediates information transfer from receptor assemblies into NF-kappaB. Sci. Adv 7, eabi9410. 10.1126/sciadv.abi9410. [PubMed: 34301608]

44. Kawai T, and Akira S (2007). TLR signaling. Semin. Immunol 19, 24–32. 10.1016/j.smim.2006.12.004. [PubMed: 17275323]

45. Alves BN, Tsui R, Almaden J, Shokhirev MN, Davis-Turak J, Fuji-moto J, Birnbaum H, Ponomarenko J, and Hoffmann A (2014). Ikap-paBepsilon is a key regulator of B cell expansion by providing negative feedback on cRel and RelA in a stimulus-specific manner. J. Immunol 192, 3121–3132. 10.4049/jimmunol.1302351. [PubMed: 24591377]

46. Peng B, Ling J, Lee AJ, Wang Z, Chang Z, Jin W, Kang Y, Zhang R, Shim D, Wang H, et al. (2010). Defective feedback regulation of NF-kappaB underlies Sjogren's syndrome in mice with mutated kappaB enhancers of the IkappaBalpha promoter. Proc. Natl. Acad. Sci. USA 107, 15193–15198. 10.1073/pnas.1005533107. [PubMed: 20696914]

47. Kearns JD, Basak S, Werner SL, Huang CS, and Hoffmann A (2006). IkappaBepsilon provides negative feedback to control NF-kappaB oscillations, signaling dynamics, and inflammatory gene expression. J. Cell Biol 173, 659–664. 10.1083/jcb.200510155. [PubMed: 16735576]

48. Paszek P, Ryan S, Ashall L, Sillitoe K, Harper CV, Spiller DG, Rand DA, and White MRH (2010). Population robustness arising from cellular heterogeneity. Proc. Natl. Acad. Sci. USA 107, 11644–11649. 10.1073/pnas.0913798107. [PubMed: 20534546]

49. O'Dea EL, Barken D, Peralta RQ, Tran KT, Werner SL, Kearns JD, Levchenko A, and Hoffmann A (2007). A homeostatic model of IkappaB metabolism to control constitutive NF-kappaB activity. Mol. Syst. Biol 3, 111.10.1038/msb4100148. [PubMed: 17486138]

50. De Lorenzi R, Gareus R, Fengler S, and Pasparakis M (2009). GFP-p65 knock-in mice as a tool to study NF-kappaB dynamics in vivo. Genesis 47, 323–329. 10.1002/dvg.20468. [PubMed: 19263497]

51. Seki T, Yamamoto M, Taguchi Y, Miyauchi M, Akiyama N, Yamaguchi N, Gohda J, Akiyama T, and Inoue J.i. (2015). Visualization of RelB expression and activation at the single-cell level during dendritic cell maturation in Relb-Venus knock-in mice. J. Biochem 158,485–495. 10.1093/jb/mvv064. [PubMed: 26115685]

52. Siggers T, Chang AB, Teixeira A, Wong D, Williams KJ, Ahmed B, Ragoussis J, Udalova IA, Smale ST, and Bulyk ML (2011). Principles of dimer-specific gene regulation revealed by a comprehensive characterization of NF-κB family DNA binding. Nat. Immunol 13, 95–102. [PubMed: 22101729]

53. Sheu K, Luecke S, and Hoffmann A (2019). Stimulus-specificity in the Responses of Immune Sentinel Cells. Curr. Opin. Syst. Biol 18, 53–61. 10.1016/j.coisb.2019.10.011. [PubMed: 32864512]

54. Sanjabi S, Williams KJ, Saccani S, Zhou L, Hoffmann A, Ghosh G, Gerondakis S, Natoli G, and Smale ST (2005). A c-Rel subdomain responsible for enhanced DNA-binding affinity and selective gene activation. Genes Dev. 19, 2138–2151. 10.1101/gad.1329805. [PubMed: 16166378]

55. Paal K, Baeuerle PA, and Schmitz ML (1997). Basal transcription factors TBP and TFIIB and the viral coactivator E1A 13S bind with distinct affinities and kinetics to the transactivation domain of NF-kappaB p65. Nucleic Acids Res. 25, 1050–1055. 10.1093/nar/25.5.1050. [PubMed: 9023117]

56. Sheppard KA, Rose DW, Haque ZK, Kurokawa R, Mclnerney E, Westin S, Thanos D, Rosenfeld MG, Glass CK, and Collins T (1999). Transcriptional activation by NF-kappaB requires multiple coactivators. Mol. Cell Biol 19, 6367–6378. 10.1128/MCB.19.9.6367. [PubMed: 10454583]

57. Zhong H, May MJ, Jimi E, and Ghosh S (2002). The phosphorylation status of nuclear NF-kappa B determines its association with CBP/p300 or HDAC-1. Mol. Cell 9, 625–636. 10.1016/s1097-2765(02)00477-x. [PubMed: 11931769]

58. Martin EW, and Sung MH (2018). Challenges of Decoding Transcription Factor Dynamics in Terms of Gene Regulation. Cells 7, 132. 10.3390/cells7090132. [PubMed: 30205475]

59. Liu G, Zhang H, Zhao C, and Zhang H (2020). Evolutionary History of the Toll-Like Receptor Gene Family across Vertebrates. Genome Biol. Evol 12, 3615–3634. 10.1093/gbe/evz266. [PubMed: 31800025]

60. Abe T, Kiyonari H, Shioi G, Inoue KI, Nakao K, Aizawa S, and Fujimori T (2011). Establishment of conditional reporter mouse lines at ROSA26 locus for live cell imaging. Genesis 49, 579–590. 10.1002/dvg.20753. [PubMed: 21445964]

61. Chalfoun J, Majurski M, Dima A, Halter M, Bhadriraju K, and Brady M(2016). Lineage mapper: A versatile cell and particle tracker. Sci. Rep 6, 36984. 10.1038/srep36984. [PubMed: 27853188]

62. Zhang Z, Ohto U, Shibata T, Taoka M, Yamauchi Y, Sato R, Shukla NM, David SA, Isobe T, Miyake K, and Shimizu T (2018). Structural Analyses of Toll-like Receptor 7 Reveal Detailed RNA Sequence Specificity and Recognition Mechanism of Agonistic Ligands. Cell Rep. 25, 3371–3381.e5. 10.1016/j.celrep.2018.11.081. [PubMed: 30566863]

63. Zhang Z, Ohto U, Shibata T, Krayukhina E, Taoka M, Yamauchi Y, Tanji H, Isobe T, Uchiyama S, Miyake K, and Shimizu T (2016). Structural Analysis Reveals that Toll-like Receptor 7 Is a Dual Receptor for Guanosine and Single-Stranded RNA. Immunity 45, 737–748. 10.1016/j.immuni.2016.09.011. [PubMed: 27742543]

64. Olguín Y, Villalobos P, Carrascosa LG, Young M, Valdez E, Le-chuga L, and Galindo R (2013). Detection of flagellin by interaction with human recombinant TLR5 immobilized in liposomes. Anal. Bioanal. Chem 405, 1267–1281. 10.1007/s00216-012-6523-4. [PubMed: 23180076]

Highlights

- Co-imaging of NF-κB RelA and c-Rel captures subunit-specific immune signaling

- The correlation of signaling between the two subunits depends on the ligand

- Ligand discrimination is more precise through signaling features of both subunits

- Mathematical modeling suggests roles of IκBs in subunit-specific ligand encoding
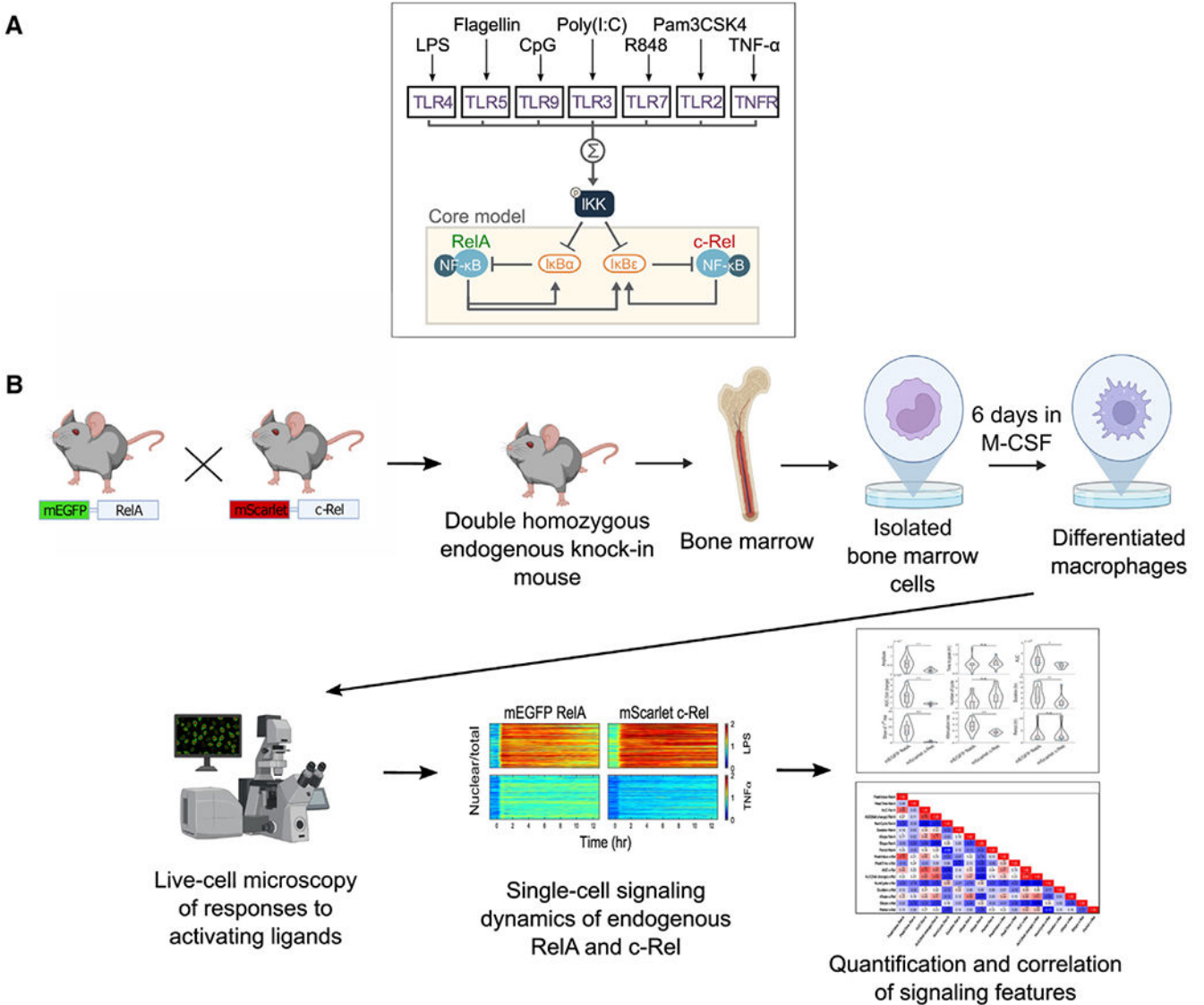
Figure 1. Schematic workflow for simultaneous live-cell imaging and analysis of both RelA and c-Rel NF-κB subunits in primary BMDM cells following stimulation with TLR ligands and TNF-α

(A) A simplified schematic of ligand recognition by different TLRs and TNF receptors (TNFRs), initiating downstream responses where NF-κB is a primary signalencoding effector. RelA and c-Rel are the two canonical subunits of the NF-κB family that mediate TLR and TNF responses.

(B) Primary BMDM cells were prepared using a standardized isolation and differentiation protocol from double-knockin endogenous NF-κB reporter mice. Both RelA and c-Rel are fluorescently labeled at their respective endogenous loci in the mice. In addition, double homozygotes are used to ensure complete labeling of the endogenous proteins. A panel of TLR ligands and a pro-inflammatory cytokine, TNF-α, were used to stimulate primary BMDMs in this study. Time lapse live-cell microscopy data were obtained and subject to

quantification and analysis workflow for the characterization of signaling dynamics of the two NF-κB subunits.
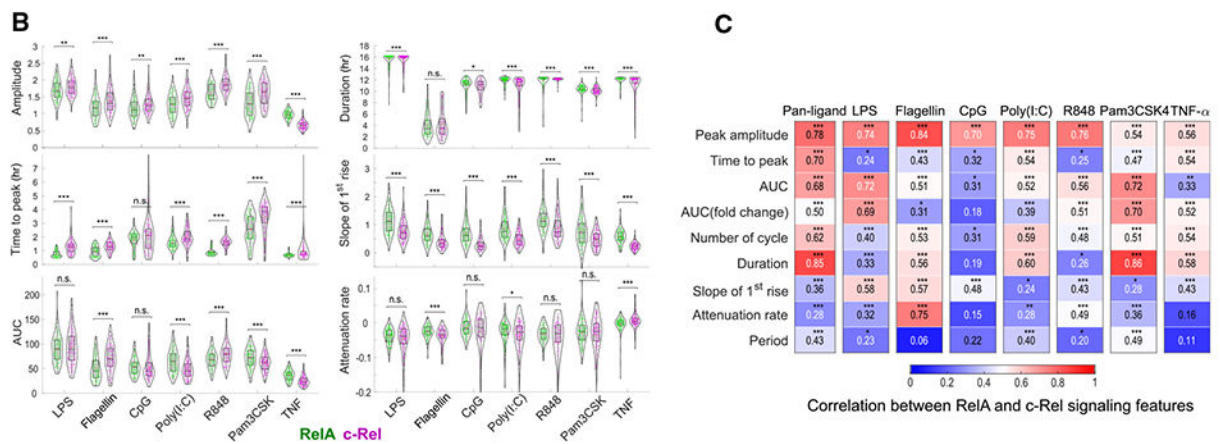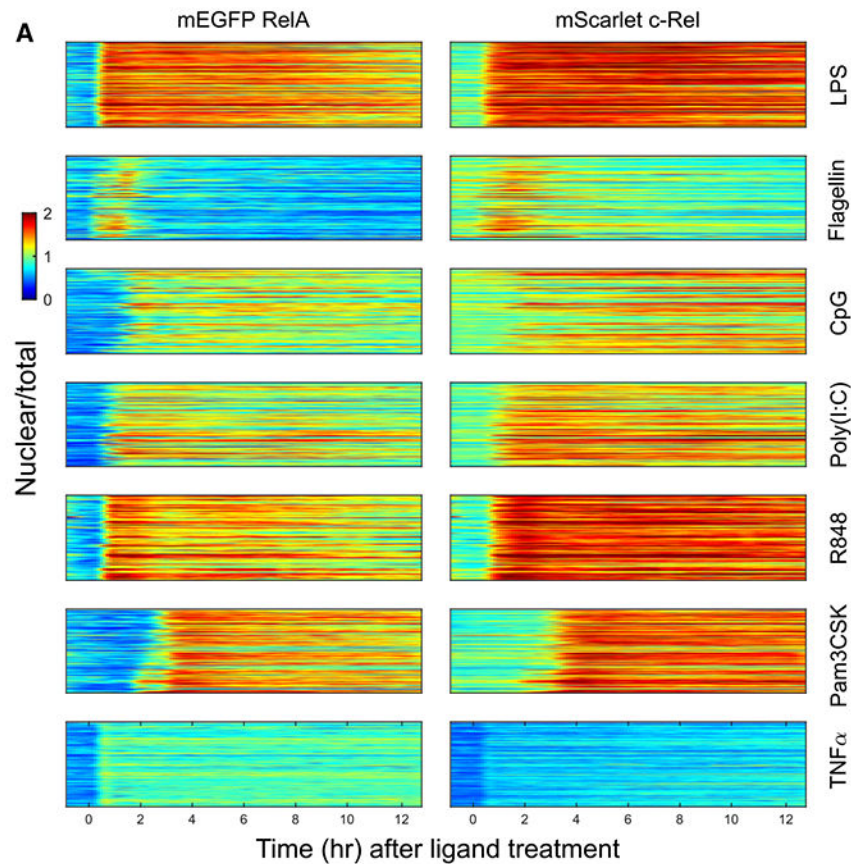
Figure 2. Quantitative imaging of RelA and c-Rel in live macrophages captures the subunit-specific signaling features for different ligands

(A) Primary BMDM cells (n = 131 for LPS, n = 112 for Flagellin, n = 118 for CpG, n = 140 for poly(I:C),n = 96 for R848, n = 109 for Pam3CSK4, and n = 109 for TNF-α) from the young green-red double-knockin reporter mice (9 weeks of age, male) were plated in a fibronectin-coated, glass-bottom 8-well imaging slide. Cells were stained with the nuclear dye SPY650-DNA 1 h before the start of imaging and treated with optimum stimulatory concentrations of six TLR ligands along with TNF-α at t = 0. Three fluorescent channels were acquired at 7 min intervals for more than 12 h. The images were processed using

custom-written MATLAB scripts. The individual rows in the heatmap show single-cell trajectories of the nuclear-to-total mean intensity ratio of RelA (left) and c-Rel (right) foreach ligand indicated on the right. The data are representative of three individual biological replicates (using independent BMDM batches from different mice on different days).

(B) Comparison of six signaling features between RelA and c-Rel signal for the data in (A). $*p < 0.05$, $**p < 0.01$, and $***p < 0.001$ from Mann-Whitney U-test.

(C) The correlation of signaling features between RelA and c-Rel depends on the activating ligand. The heatmap displays the Pearson correlation coefficients between RelA and c-Rel signaling features extracted from time series data for each ligand. Each column is from the indicated ligand. The individual correlation coefficient values are shown within each cell, and the asterisk (*) denotes the statistical significance, where $*p < 0.05$, $**p < 0.001$, and $***p < 0.0001$. Data are representative of three independent biological replicates (using independent BMDM batches from different mice on different days).
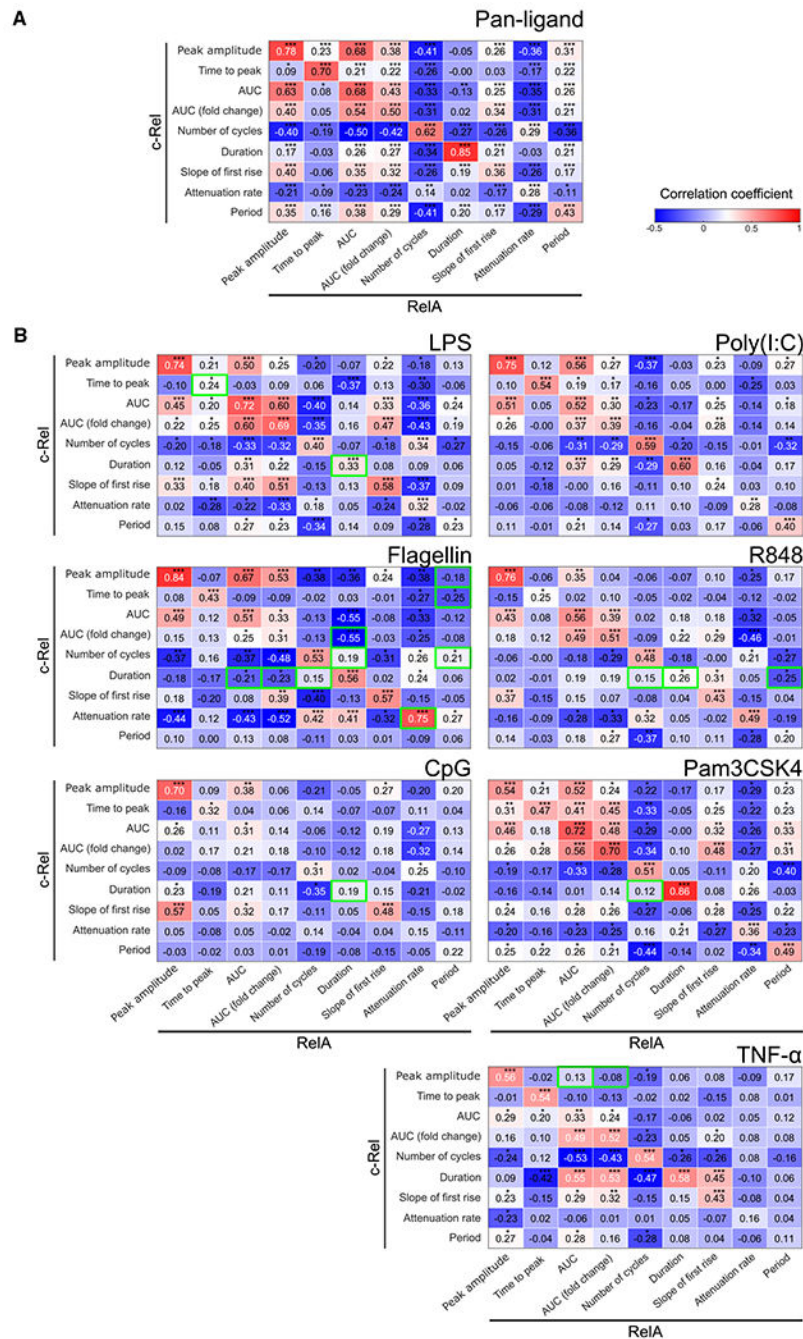
Figure 3. Cross-correlations of signaling features reveal the sources of RelA and c-Rel divergence in encoding ligand specificity

(A) The pan-ligand cross-correlation matrix was generated by calculating the Pearson correlation coefficients between all possible pairs of signaling features between RelA and c-Rel. The entire single-cell time series imaging data were used from all ligands. The individual correlation coefficient values are shown within each cell, and the asterisk (*) denotes the statistical significance, where *p < 0.05, **p < 0.001, and ***p < 0.0001.

(B) The ligand-specific cross-correlation matrix was similarly generated except by using imaging data for the indicated ligand only. The diagonal of each matrix corresponds to

the column for the indicated ligand in Figure 2C. The green boxes around the cells in the matrix represent the correlations that are different (at least 0.45 absolute difference) from the pan-ligand correlation matrix. The data are representative of three individual biological replicates (using independent BMDM batches from different mice on different days).
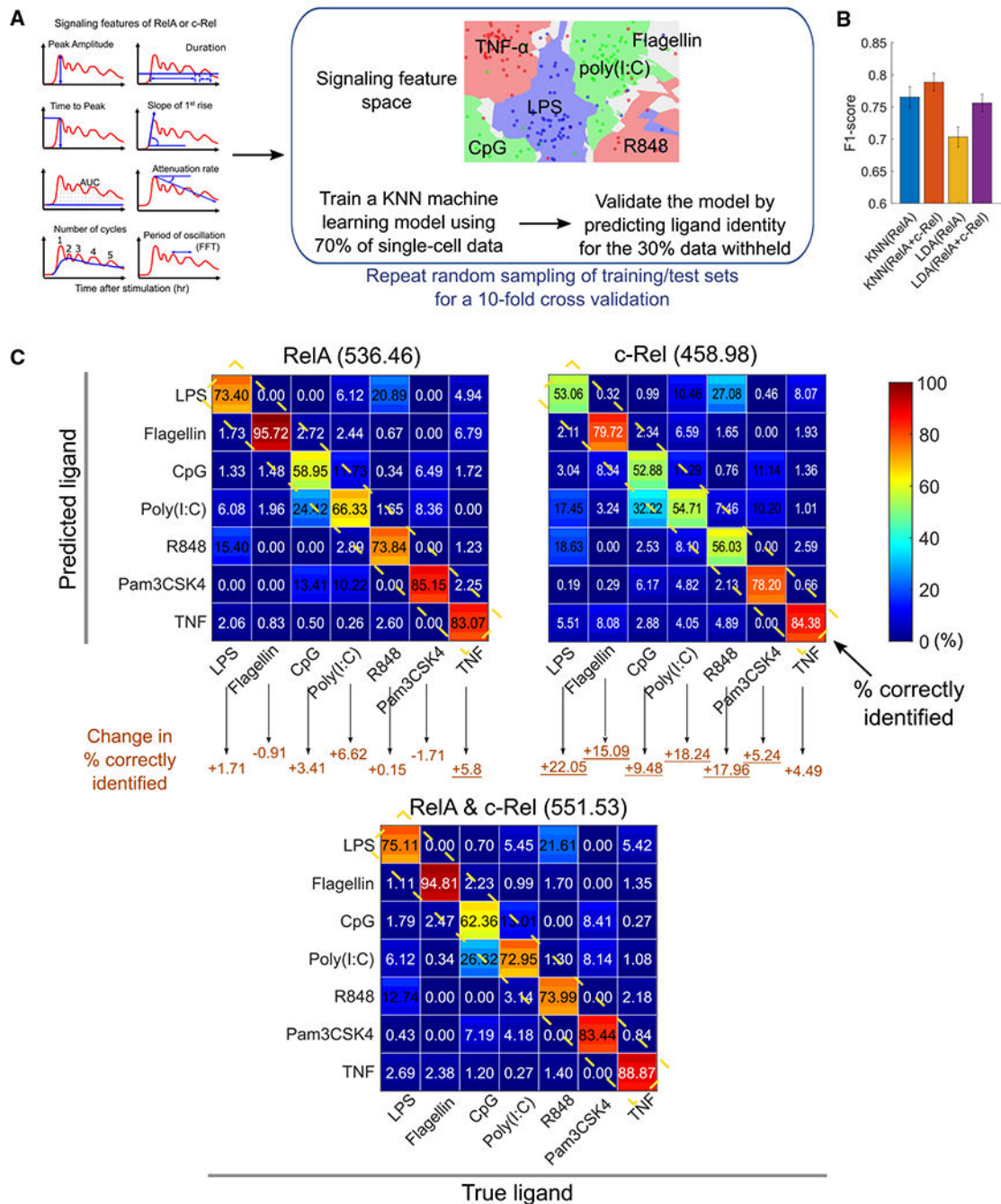
Figure 4. The signaling features of both NF-κB subunits can distinguish immune threats better than those of either subunit alone

(A) Computational workflow of supervised machine learning (ML)with K-nearest neighbor (KNN) models that learn features from RelA alone or from both RelA and c-Rel and predict ligand identity. Models were created by randomly selecting 70% of data for training; the remaining 30% of data were used for testing with a 10-fold cross-validation.

(B) The average F1 scores of ligand predictions using either the RelA signaling features only or both RelA and c-Rel signaling features, produced by the KNN or the linear discriminant

analysis (LDA) methods. The F1 scores are shown here with mean ± standard error from a 10-fold cross-validation.

(C) Confusion matrices show the performance of KNN ML models (K = 7, Canberra distance) using the signaling features of RelA (top left), c-Rel (top right), or both RelA and c-Rel (bottom). Within each cell of the matrix, the colors within the subrectangles above and below the numerical value (mean of the 10-fold cross-validation in B) represent the upper and lower bounds (95% confidence interval). The sum of diagonals (percentage correctly identified) for each matrix is shown in parentheses. The statistically significant changes between components of an upper matrix and a lower matrix are underlined (p < 0.05 in Mann-Whitney U test). The results are representative of three individual biological replicates (using independent BMDM batches from different mice on different days).
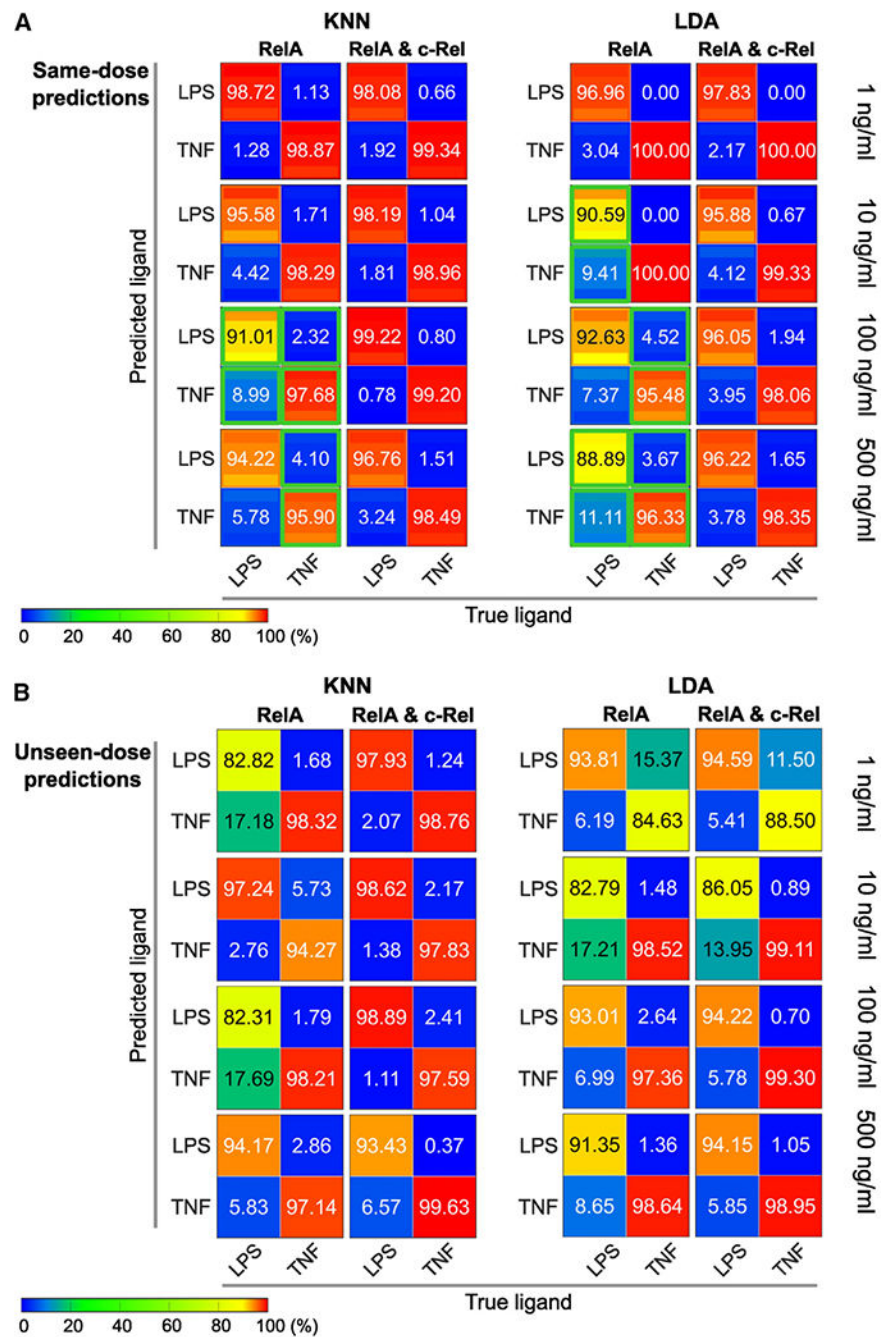
Figure 5. Signaling features of c-Rel help maintain ligand discrimination at high doses

Primary BMDM cells from a young male green-red double-knockin reporter mouse (11 week of age) were imaged for their responses to LPS or TNF-α at the indicated concentrations. The dynamic features of RelA and c-Rel were quantified and analyzed (numbers of single cells analyzed: n = 154, 113, 127, and 149 for 1, 10, 100, and 500 ng/mL LPS; n = 267, 265, 212, and 266 for 1, 10, 100, and 500 ng/mL TNF-α).

(A) For each dose, models were created by randomly selecting 70% of data for training; the remaining 30% of data were used for testing with a 10-fold cross-validation. The 2 ×

2 confusion matrices show the performance of ML models, KNN with K = 7, Canberra distance (left), and LDA (right), using the signaling features of RelA, or both RelA and c-Rel, for a given dose. Within each cell of the matrix, the colors within the subrectangles above and below the numerical value (mean of the 10-fold cross-validation) represent the upper and lower bounds (95% confidence interval). The green boxes mark the ML models with less accurate predictions using RelA features only that undergo statistically significant improvements in predictions by using features of both subunits ($p < 0.05$ in Mann-Whitney U test).

(B) ML models were trained with the signaling features extracted from data for the indicated concentration shown on the right. Each dose-specific model was tested against the remaining data from all the other doses. The confusion matrices show the performance of ML models, KNN with K = 7, Canberra distance (left), and LDA (right), using the signaling features of RelA or both RelA and c-Rel. The colormap was chosen to aid the visualization of changes in the 80%–100% range. The results are from one of two biological replicates (using independent BMDM batches from different mice on different days).
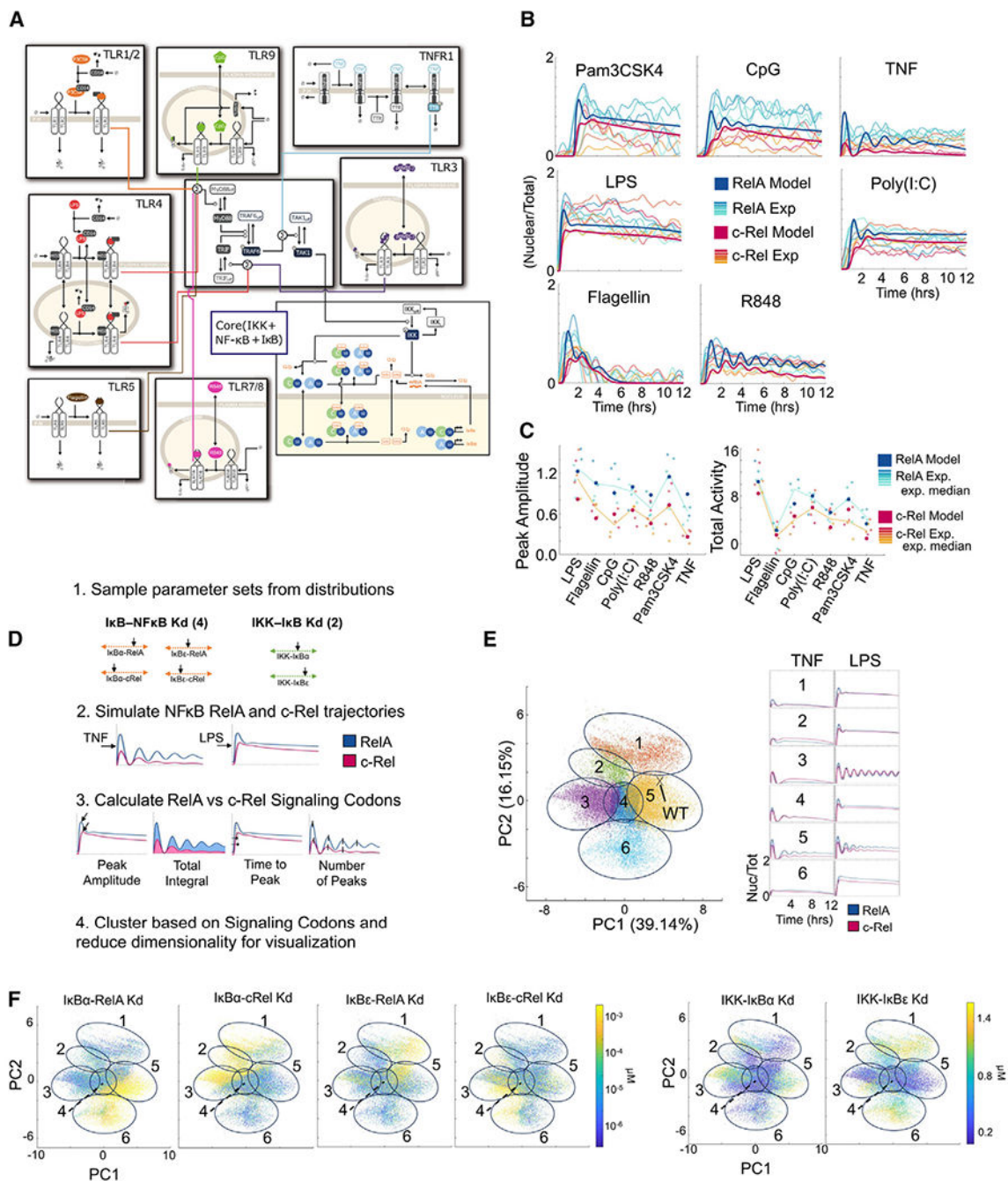
Figure 6. Mathematical modeling of the TLR-NF-κB signaling network recapitulates stimulus-responsive RelA and c-Rel dynamics

(A) The topology of the model that combines seven receptor-proximal signaling modules with a core NF-κB module that includes both RelA-and c-Rel-containing NF-κB dimers and both IκBα and IκBε. See STAR Methods for details. In the core module, A: RelA, C: c-Rel, 50: p50.

(B) Simulated nuclear abundances (relative to total) of RelA- (blue) and c-Rel- (red) containing NF-κB dimers are shown as bold curves. Lighter color curves indicate five representative single-cell trajectories from imaging data of Figure 2.

(C) Plots of peak amplitude (maximum value within first 4 h) and total activity (integral over complete time series) extracted from the experimental NF-κB trajectories and from model simulations.

(D) Workflow for parameter set variation to identify determinants of RelA and c-Rel dynamic trajectories.

(E) PCA (principal-component analysis) of 100,000 parameter sets defined by their differences in RelA and c-Rel signaling codons in response to TNF-α and LPS stimulation (left). Parameter sets colored by cluster identity and WT (wild-type) parameter set marked. Representative parameter set (smallest distance to cluster mean) simulations from each cluster (right).

(F) PCA colored by values for the indicated interaction parameters.
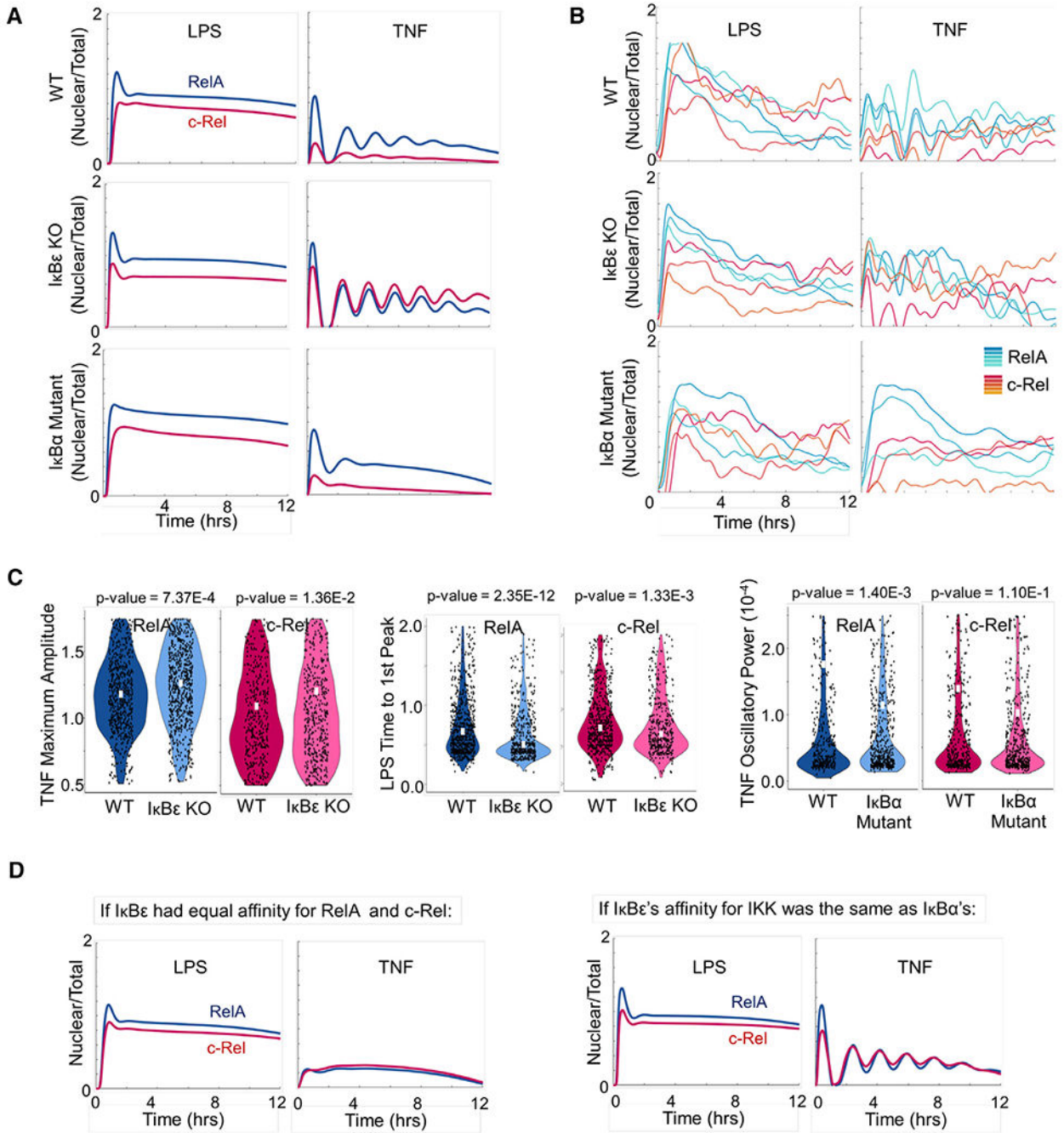
Figure 7. RelA and c-Rel dynamics from IκB signaling mutants support model predictions

(A) Mathematical model predictions of RelA and c-Rel response dynamics to LPS and TNF-α stimulation in IκBε KO (middle) and IκBα mutant (bottom) cells.

(B) Representative experimental trajectories of RelA and c-Rel in response to LPS and TNF-α stimulation in WT, IκBε KO,[27] and IκBα mutant.[46]

(C) Violin plots of peak amplitude (left) in response to TNF-α of experimental RelA and c-Rel trajectories in IκBε KO, time to first peak (middle) in response to LPS, and oscillatory power (right) in response to TNF-α (average power within the biologically relevant 0.33–1

h^{-1} frequency range from power spectral density estimate of signal) of RelA and c-Rel experimental trajectories in IκBα mutant. White boxes denote median values.

(D) Mathematical model simulations of RelA and c-Rel trajectories in response to LPS and TNF-α stimulation when IκBε affinity to RelA is set equivalent to that of c-Rel (left) and IKK affinity to IκBε is set equivalent to that of IκBα (right). The experimental results for RelA dynamics are consistent with three replicates in response to multiple ligand stimulations.[7]
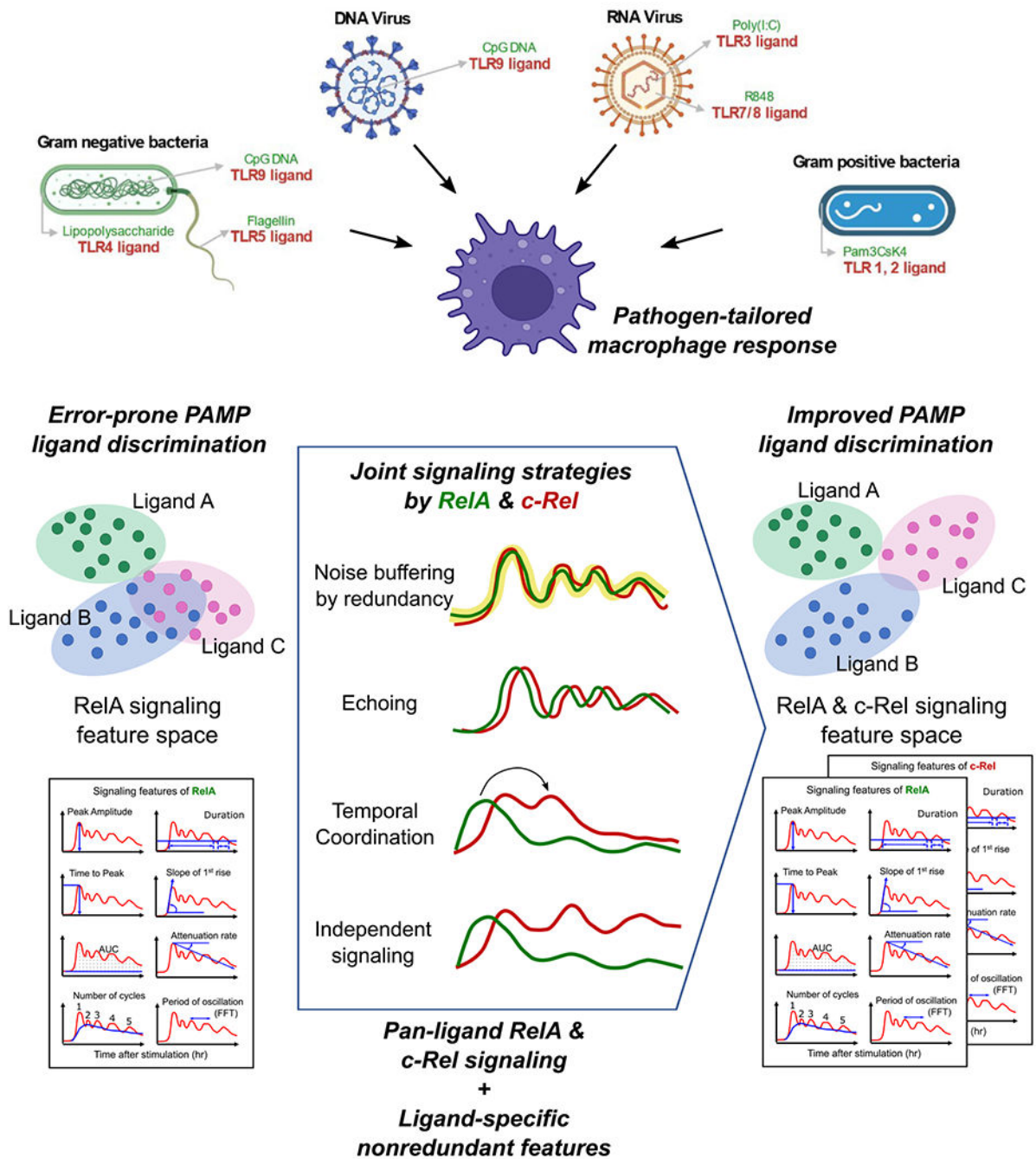
Figure 8. Ligand discrimination by joint signaling of two NF-κB subunits
Some concepts and results of the study are illustrated. PAMPs are recognized by different TLRs as activating ligands, initiating complex kinetic responses of downstream transcription factors. Live-cell imaging of co-signaling dynamics showed unexpectedly non-redundant behaviors of the two subunits, RelA and c-Rel, of NF-κB that underlie an enhanced PAMP ligand discrimination in macrophages.

REAGENT or RESOURCE	SOURCE	IDENTIFIER
caret	Max Kuhn	https://cran.r-project.org/web/packages/caret/index.html
lattice	Deepayan Sarkar	https://cran.r-project.org/web/packages/lattice/index.html
MASS	W. N. Venables and B. D. Ripley	https://cran.r-project.org/web/packages/MASS/index.html
NF-κB signaling network model & simulation code	This paper	https://github.com/apekshasingh/Rela_cRel_Model
Other		
Cell strainers	Fisher Scientific	Cat# 22-363-548
μ-Slide 8 Well chamber slide	Ibidi	Cat# 80826